NATIONAL AERONAUTICS AND SPACE ADMINISTRATION

N70-28943

Space Programs Summary 37-62, Vol. I

Flight Projects

For the Period January 1 to February 28, 1970

CASE FILE COPY

NASA FILE COPY
Return to
NASA HQ LIBRARY (USS-10)
WASHINGTON, D.C. 20546 STOP 85
HQ. LIBRARY (USS-10)

JET PROPULSION LABORATORY
CALIFORNIA INSTITUTE OF TECHNOLOGY
PASADENA, CALIFORNIA

March 31, 1970

NATIONAL AERONAUTICS AND SPACE ADMINISTRATION

Space Programs Summary 37-62, Vol. I

Flight Projects

For the Period January 1 to February 28, 1970

JET PROPULSION LABORATORY
CALIFORNIA INSTITUTE OF TECHNOLOGY
PASADENA, CALIFORNIA

March 31, 1970

SPACE PROGRAMS SUMMARY 37-62, VOL. I

Copyright © 1970
Jet Propulsion Laboratory
California Institute of Technology

Prepared Under Contract No NAS 7-100
National Aeronautics and Space Administration

Preface

The Space Programs Summary is a multivolume, bimonthly publication that presents a review of technical information resulting from current engineering and scientific work performed, or managed, by the Jet Propulsion Laboratory for the National Aeronautics and Space Administration The Space Programs Summary is currently composed of four volumes

Vol I	*Flight Projects* (Unclassified)
Vol II	*The Deep Space Network* (Unclassified)
Vol III	*Supporting Research and Advanced Development* (Unclassified)
Vol IV	*Flight Projects and Supporting Research and Advanced Development* (Confidential)

"Page missing from available version"

IV.

Contents

I. *Mariner* Mars 1971 Project 1

A Project Description and Status 1

1 Description 1

2 Status 3

B Space Sciences 4

1 Television Subsystem 4

C. *Engineering Mechanics* 7

1 Introduction 7

2 Propulsion Support Structure 7

3 Flight Cabling 11

4 Thermal Resistance at Chassis–Subchassis Interface 11

5 DTM Static Test 12

6 Spacecraft Modal Survey 16

7 Spacecraft Overturning Moment for Longitudinal Low-Frequency Environmental Vibration Test 17

8 Metallurgical Study of Burst-Tested Propellant Vessel 18

9 Electronic Parts Control 19

D Propulsion 22

1 Propulsion Subsystem 22

II. *Viking* Project, Orbiter System and Project Support 27

A Project Description and Status 27

1 Description 27

2 Status 28

B Space Sciences 28

1 Dynamic Response of a Gas Chromatograph–Mass Spectrometer Combination 28

C Guidance and Control 33

1 Effects of Propellant Slosh Dynamics on *Viking* Orbiter Powered Flight Control 33

D Engineering Mechanics 35

1 Introduction 35

2 Configuration Description 36

Contents (contd)

3 Electronic Equipment Layout 39

4 Solar Energy Controllers 41

Subject Index 45

I. *Mariner* Mars 1971 Project

A. Project Description and Status

1. Description

The primary objective of the *Mariner* Mars 1971 Project is to place two spacecraft in orbit around Mars that will be used to perform scientific experiments directed toward achieving a better understanding of the physical characteristics of that planet Principal among these experiments are measurements of atmospheric and surface parameters at various times and locations to determine the dynamic characteristics of the planet Approximately 70% of the Martian surface will be observed during a minimum of 90 days of orbital operations

During Mission A, it is planned to map the topography of a large portion of the Martian surface at a resolution significantly higher than that achievable with earth-based methods or by the *Mariner* Mars 1969 spacecraft In addition, measurements will be made of the composition, density, pressure, and thermal properties of the planet's atmosphere Other measurements will be directed toward an understanding of Mars' surface temperatures, composition, and thermal properties (particularly at the polar caps), its apparent lack of internal activity, its mass distribution, and its shape

During Mission B, data will be sought on time-variable features of the Martian surface associated with the wave of darkening wherein both seasonal and secular changes occur Also, information on atmospheric structure and gross dynamics will be obtained, as well as information directed toward an understanding of Mars' mass distribution, its shape, and its apparent lack of internal activity

A capability will exist to redirect goals for either mission to the alternate mission if desired The two launches are anticipated for May 1971, with arrival at the planet during the following November

An engineering objective of the project is to demonstrate the ability of the spacecraft to perform orbital operations in an adaptive mode wherein information from one orbital pass is used to develop the operations plan for subsequent orbital passes Studies indicate a high probability that at least one of the spacecraft will survive the sun occultation period which occurs shortly after the 90-day mission is

completed This makes it possible to conduct an Extended Mission for about a year after orbit insertion The Extended Mission will probably consist of one or two data taking sequences per week with the capability of recording and playing back about a half-recorder of data (16 TV frames and 11 min of spectrometer data)

One of the *Mariner* Mars 1971 flight spacecraft will be new, and the other will be the spare flight spacecraft of the *Mariner* Mars 1969 Project modified to meet the requirements of the 1971 missions and to enhance mission reliability The proof test model spacecraft of the *Mariner* Mars 1969 Project will be modified to become the proof test model for the *Mariner* Mars 1971 Project, to be used for preliminary testing and as a simulator in support of flight operations A major modification for the *Mariner* Mars 1971 mission will be the addition of a rocket motor required to decelerate the spacecraft and place it in orbit around Mars

Separate scientific instrument subsystems will be required to accomplish the television, infrared radiometer, ultraviolet spectrometer, and infrared spectrometer interferometer experiments given in Table 1 The S-band occultation and celestial mechanics experiments will require no additional equipment on the spacecraft.

Management responsibilities for the overall project, the Spacecraft System, the Mission Operations System, and the Tracking and Data System have been assigned to JPL

Table 1. *Mariner* Mars 1971 scientific experiments and principal investigators

Television	
H Masursky	Team leader
H Masursky	PI/U S Geological Survey
R Batson	CI/U S Geological Survey
W Borgeson	
M Carr	
J F McCauley	
D Milton	
R Wildey	
D Wilhelms	
J Lederberg	PI/Stanford University
E Levinthal	CI/Stanford University
J B Pollack	CI/Cornell University
C Sagan	CI/Cornell University
G de Vaucouleurs	PI/University of Texas
W B Thompson	PI/Bellcomm
G A Briggs	CI/Bellcomm
P L Chandeysson	CI/Bellcomm
E N Shipley	CI/Bellcomm
B Smith	PI/New Mexico State University
M E Davies	CI/Rand Corp
W K Hartmann	CI/Arizona State University
N H Horowitz	CI/Caltech
R B Leighton	CI/Caltech
C B Leovy	CI/University of Washington
T B McCord	CI/MIT
B C Murray	CI/Caltech
R P Sharp	CI/Caltech
Ultraviolet spectrometer	
C Barth	PI/University of Colorado
C W Hord	CI/University of Colorado
J B Pearce	CI/University of Colorado
Infrared interferometer spectrometer	
R A Hanel	PI/Goddard Space Flight Center
B J Conrath	CI/Goddard Space Flight Center
W A Hovis	CI/Goddard Space Flight Center
V Kunde	CI/Goddard Space Flight Center
G V Levin	CI/Biospherics
P D Lowman	CI/Goddard Space Flight Center
C Prabhakara	CI/Goddard Space Flight Center
B Schlachman	CI/Goddard Space Flight Center
Infrared radiometer	
G Neugebauer	PI/Caltech
S C Chase	CI/Santa Barbara Research Center
H Kieffer	CI/UCLA
E D Miner	CI/JPL
G Munch	CI/Caltech
Celestial mechanics	
J Lorell	Team leader
J Lorell	PI/JPL
J D Anderson	CI/JPL
W L Martin	CI/JPL
W L Sjogren	CI/JPL
I Shapiro	PI/MIT
M Ash	CI/MIT
W Smith	CI/MIT
S-band occultation	
A Kliore	PI/JPL
D L Cain	CI/JPL
G Fjeldbo	CI/JPL
B L Seidel	CI/JPL

PI = Principal investigator, who is the proposer for each experiment

CI = Co-investigator, who assists the proposer on each experiment

Team leader heads a particular group of PIs and CIs on an experiment where there is more than one PI

Lewis Research Center has been assigned management responsibility for the Launch Vehicle System The launch vehicle will be an *Atlas/Centaur* developed by General Dynamics/Convair

The *Mariner* Mars 1971 missions will be supported by the Air Force Eastern Test Range launch facilities at Cape Kennedy, the tracking and data acquisition facilities of the Deep Space Network, and other NASA facilities

2 Status

Project activities were concentrated on reassessing and reducing FY 1970 expenditures Extensive budget reviews were made at NASA, JPL, and at the contractors Revised plans and tighter cost control procedures were implemented

Spacecraft System efforts included assembly and testing of proof test model (PTM) equipment at the subsystem level Results of the final calibration test of the radio PTM subsystem have been excellent to date The ultraviolet spectrometer PTM is undergoing environmental tests, an engineering model battery was environmentally tested, and the propulsion engineering model is in final assembly

The Tracking and Data System test plan was published The JPL Scientific Computing Facility dual-processor 1108 was split into two single-processor 1108s One of the single-processors will be used by the Tracking and Data System

An initial study was completed indicating a minimum periapsis altitude for Mission B of about 850 km A similar study is being undertaken for Mission A A first issue of a Science Mission Plan was published The guidance design programs are now nearly complete and the guidance analysis is beginning The most recent performance assessment indicates a 28-day launch period with a +22-lb margin The first draft of the Telecommunications Link Performance Document was issued. The Preliminary Trajectory Characteristics Document covering launch through insertion was published The launch through orbit insertion orbit determination accuracy studies were completed indicating that the initial project requirements can be met

The television team matrix was revised to include a Mission Operations Group (Fig 1).

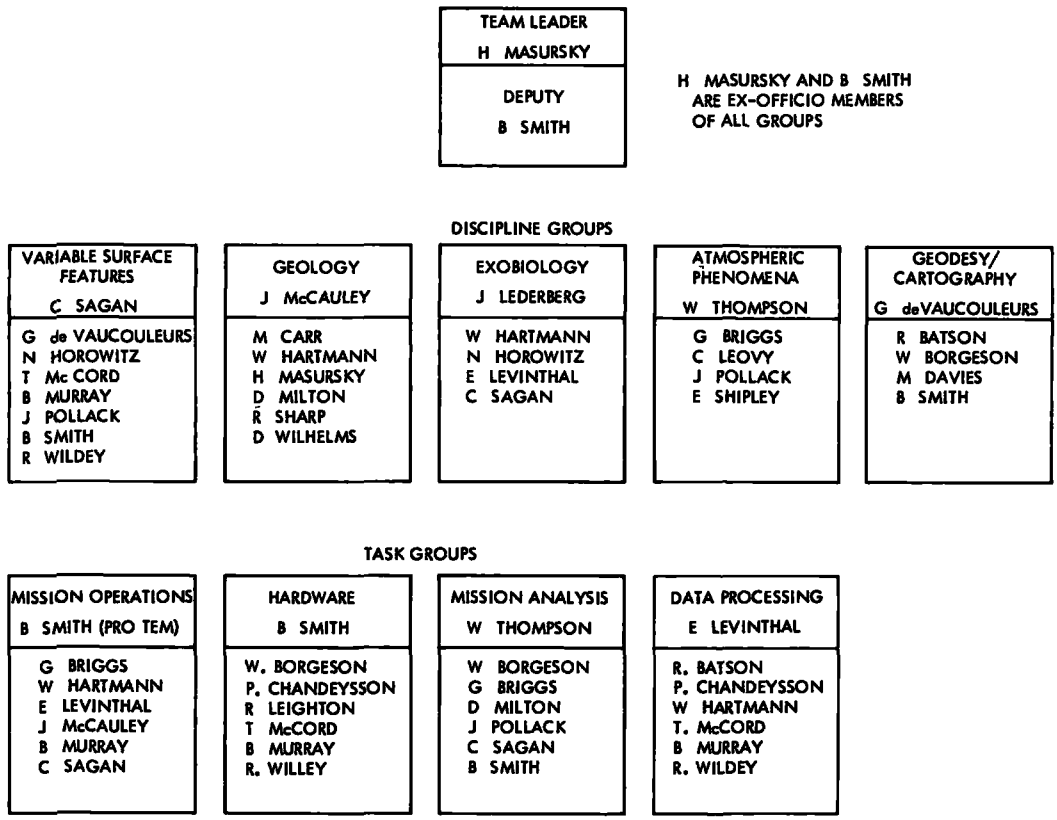

Fig. 1. Television team matrix

B. Space Sciences

1. Television Subsystem

a. Introduction. The *Mariner* Mars 1971 TV subsystem is a second generation of the TV subsystem flown on *Mariners VI* and *VII* The principal changes are adaptation of the all digital data storage subsystem, increased flexibility of shutter control and filter selection to adapt to the orbital mission, and minor modifications of the detailed design to increase the instrument reliability.

b. Instrument description. The TV subsystem (TVS) consists of two cameras mounted to the spacecraft planetary scan platform, with supporting electronics housed in the bus portion of the spacecraft. Wide- and narrow-angle optics, shutter mechanism, and some portions of the electronics are identical to the equipment developed for the *Mariner* Mars 1969 TVS.

The wide-angle camera (50-mm focal length), which has a field-of-view of 11 × 14 deg, utilizes a six-element Zeiss planar lens and is equipped with a filter wheel that can be controlled to provide any one of eight filters in the optical path This filter wheel contains both spectral and polarizing filters. The wheel can be advanced none, one, or two steps between consecutive wide-angle pictures by ground command, or will take two steps between each picture, thus cycling continuously through a four-filter sequence when in the automatic mode

The narrow-angle camera (508-mm focal length), which has a field-of-view of 1 1 × 1 4 deg, utilizes an 8-in.-diameter Schmidt–Cassegrain telescope and video processing elements identical to the wide-angle camera

Both cameras have focal-plane shutters, similar to the type used on the *Surveyor* and *Mariner* Mars 1969 TV cameras. After passing through the filter and shutter, the optical image is focused onto a slow-scan vidicon. Vidicon electron beam focus, alignment, and vertical and horizontal deflection are performed magnetically Table 2 gives some of the significant instrument parameters.

The video information is processed by the signal chain which is shown schematically in Fig 2 It consists of an ac-coupled video amplifier containing a fourth-order bandpass filter, a synchronous demodulator, followed by a fifth-order Butterworth low-pass filter. The video signal from the vidicon is converted to a modulated carrier signal by chopping the vidicon cathode current at the carrier frequency rate The carrier frequency is 28.8 kHz and

Table 2. TV subsystem functional parameters

Characteristic	Wide-angle camera	Narrow-angle camera
Focal length, mm	50	508
Focal length ratio	f/4 0	f/2 35
Fastest shutter speed, ms	3	3
Angular field-of-view, deg	11 × 14	1 1 × 1 4
Active vidicon target raster, mm	9 6 × 12 5	9 6 × 12 5
Scan lines per frame	700	700
Frame time, s	42	42
Picture elements per line	832	832
Bits per picture element	9	9
Video carrier frequency, kHz	28 8	28 8
Video baseband, kHz	7 35	7 35
Video sampling frequency, kHz	14 7	14 7

is synchronized with the spacecraft power frequency Some noise rejection is accomplished by phasing the carrier so that the vidicon beam current is off during the switching noise burst generated by the spacecraft primary ac power The low-pass filter has a bandwidth from dc to 7 35 kHz The output of this filter is sampled by a 9-bit analog-to-digital converter at a 14 7-kHz sampling rate, which provides a data stream from the TV subsystem of 832 9-bit words for each of the 700 lines comprising one TV frame The bandpass filter consists of two second-order sections with a bandwidth of 28.8 ± 7 35 kHz

The first section of the bandpass filter, along with the pre-amplifier and post-amplifier, are contained in the camera head Their function is to provide sufficient gain to raise the video signal from a maximum of about 5 nA obtained from the target electrode in the vidicon to a maximum of 5 V at the camera head output The first section of the bandpass filter provides noise rejection in the camera head by limiting the signal chain bandwidth. The remainder of the video chain is contained within Bay VII of the spacecraft bus The bus electronics consists of an ac isolation amplifier to provide common mode noise rejection at the input, the second section of the bandpass filter, the synchronous demodulator, the low-pass filter, and the analog-to-digital converter

The digital signal is transmitted to the data automation subsystem (DAS), where it is rate-buffered and formatted for input to the spacecraft tape recorder. There it is stored until it can be played back

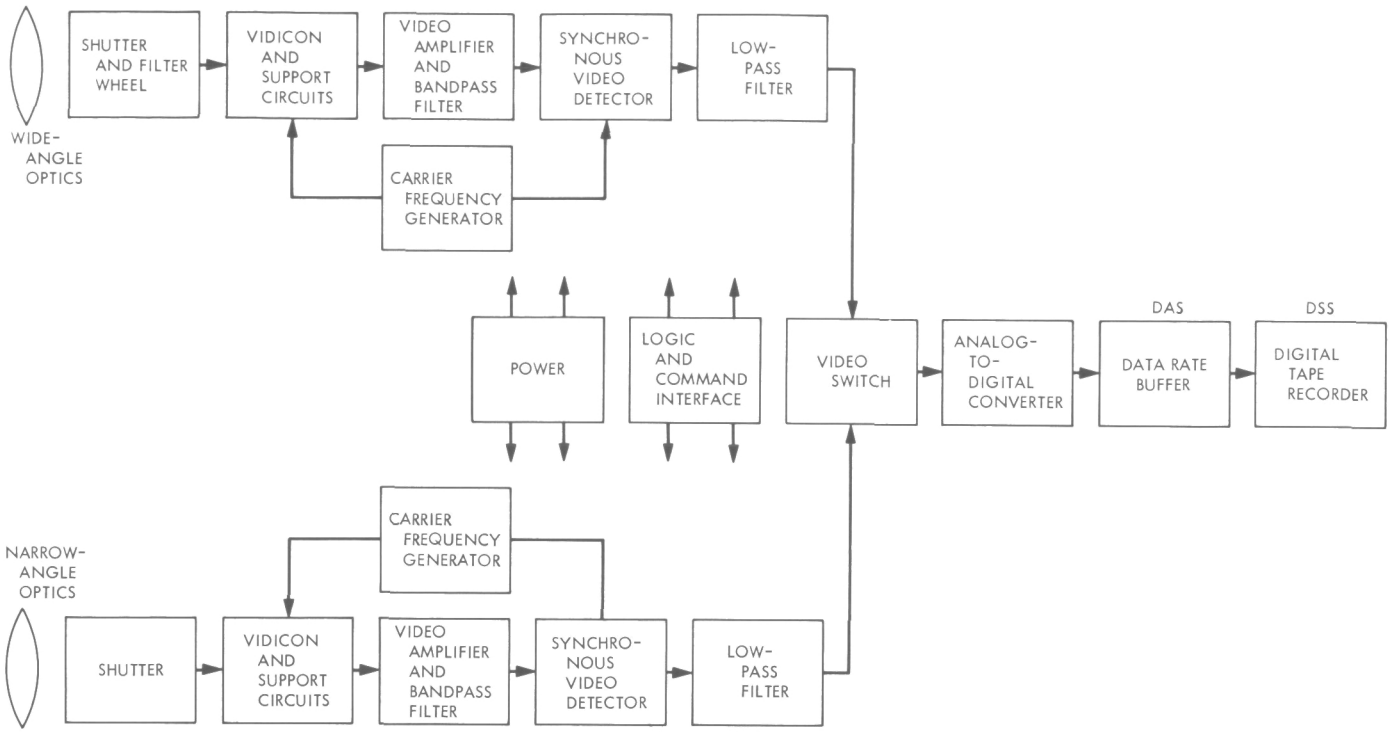

Fig. 2. *Mariner* Mars 1971 TV subsystem block diagram

In addition to buffering the TV data, the DAS supplies the various timing control functions for the TV sweep circuits, and computes the average video levels of each wide- (or narrow-) angle picture to set the vidicon exposure time for the next wide- (or narrow-) angle picture.

The resolution of planetary surface features and the planetary surface area in the field-of-view of each camera is dependent on the slant range from the cameras to the planetary surface. With the cameras pointed in the nadir direction and the spacecraft at an altitude of 1800 km, surface resolution in the wide- and narrow-angle cameras corresponds to 1 and 0.1 km, respectively.

It is possible, by ground command, to take a single wide- or narrow-angle picture, to take pictures in wide- and narrow-angle pairs at selected points on the surface, or to take a sequence (wide, narrow, wide, etc.) of pictures until the tape recorder is filled (32 pictures). In the automatic exposure control mode (without receipt of a ground command in a particular orbit), the TV picture will be recorded in a continuous wide-, narrow-angle camera sequence. In this mode, there are three brightness ranges, which are the same for both cameras, giving a total brightness range of from 11 to 2200 ft-L.

c. Breadboard description. Figure 3 illustrates the TVS breadboard in test configuration with the breadboard checkout equipment (BCE). The TVS breadboard was designed and constructed to be electrically identical to the TVS flight hardware, and mechanically similar in camera-head construction. The utilization of the breadboard is as follows:

(1) To verify both the circuit and subsystem design performance, to identify circuit and subsystem design errors and problems, and to test design fixes.

(2) To perform circuit and subsystem performance margin testing at worst-case voltage conditions over a temperature range 10°C below the lower and above the upper type-approval temperature ranges (exception was taken to this in the case of the vidicons).

(3) To establish the optimum wiring configuration for the TVS bus electronic to scan platform harness.

(4) To verify the application of all components to be used in the TVS flight hardware (certain exceptions were taken to this in the case of long lead items, notably precision resistors).

(5) To verify the correctness of flight hardware build documentation. This was accomplished by compar-

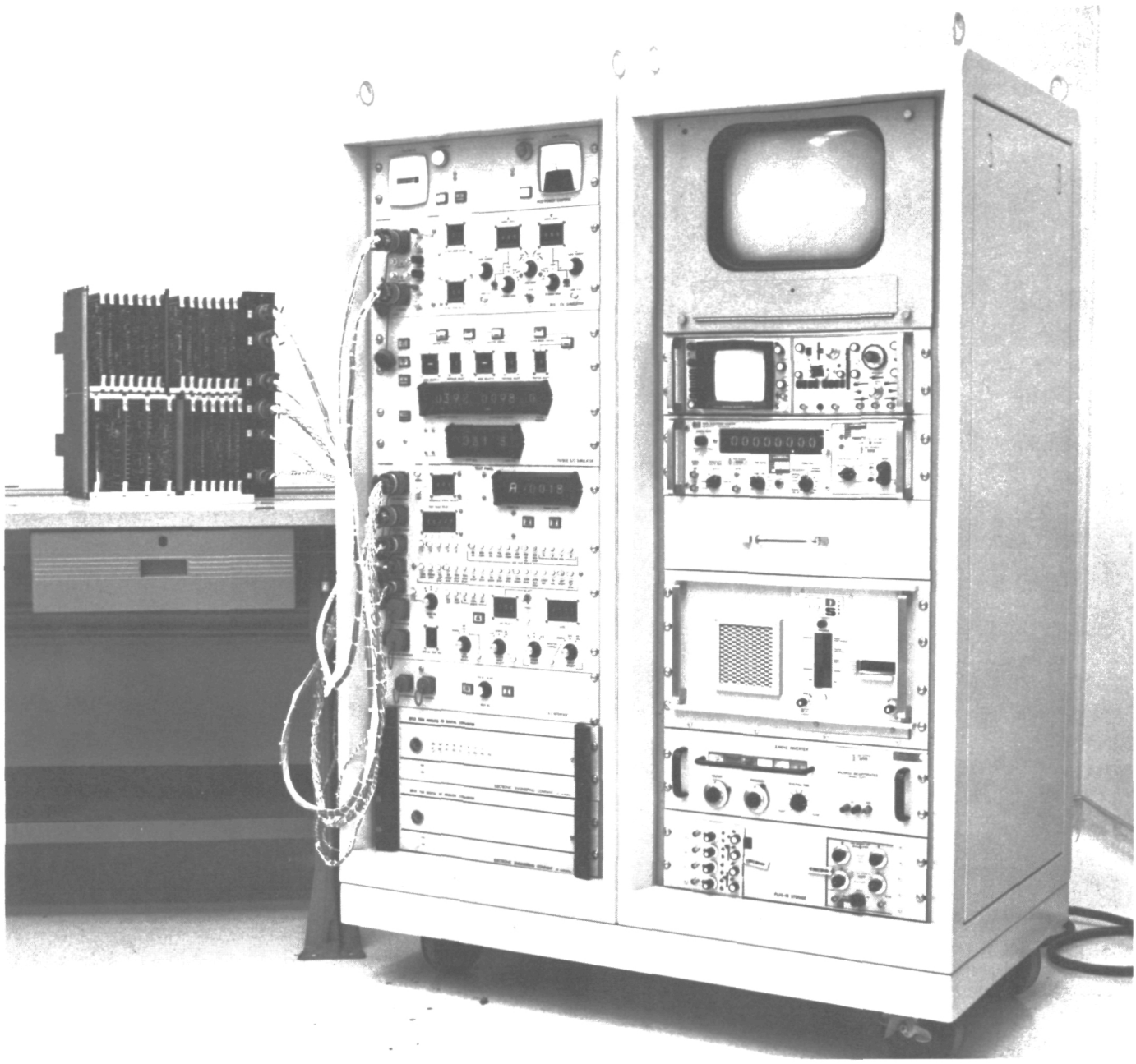

Fig. 3. TV subsystem breadboard in test configuration with BCE

ing actual breadboard circuits against released prototype schematics. A total of eight flight hardware design errors were detected, which prevented eight problems at first power application on the prototype.

(6) To verify design and performance of test fixtures to be used in testing flight hardware. To accomplish this, the breadboard mechanical design compartmentalizes the electronics the same as the flight electronics chassis does. Several problems in the test fixtures were identified in these tests; this prevented test-induced failures in the prototype TVS.

(7) To support initial checkout of the interface between the Image Processing Laboratory and the TVS-associated support equipment (digital tape recorder and BCE).

(8) To verify TVS/DAS interface compatibility.

(9) To photograph stars, Saturn, and the moon. Initial testing was conducted in January 1970, with successful photographing of Saturn and the moon. Longer exposure times were required for star shots, and a combination of fog and air turbulence negated the quantitative value of these photographs, but future testing will be conducted to definitize the capability of doing in-flight geometric calibration using star shots.

The breadboard TVS configuration will be maintained current with the flight hardware during the pre-launch period so that meaningful investigations of hardware-related problems can be accomplished without risk to flight-type equipment.

d. BCE description. The BCE provides interface simulation, TVS output display, and processing and testing of the TVS output signals. Its functions include support of TVS functional tests, TVS calibration, troubleshooting of the TVS, signal buffering between the TVS and tape recorder and the TVS and remote displays, and data buffering to the Image Processing Laboratory. All environmental testing of the TVS is done with only the BCE interfacing electrically with the TVS, so that test setups are consistent and repeatable, and to avoid the possibility of test-induced failures through ground loops with arbitrary ancillary equipment.

The BCE and major portions of the TVS were designed and are being fabricated by Electro-Optical Systems under JPL Contract 952419. The vidicon tubes being used are manufactured by General Electrodynamics Corporation.

C. Engineering Mechanics

1. Introduction

During the reporting period, the development test model structural tests were completed; the temperature control model was prepared for a series of simulator tests; and proof test model and flight equipment fabrication was continued.

2. Propulsion Support Structure

a. General description. Integral to the configuration of the *Mariner* Mars 1971 spacecraft is a large bipropellant propulsion module attached to the top of the main spacecraft structure. This propulsion module (Fig. 4) must be removable from the spacecraft as a single module to permit loading and testing independent of the spacecraft and to permit final installation near the conclusion of spacecraft systems testing.

Two 30-in.-diameter propellant tanks, two 15-in.-diameter pressurant tanks, one rocket engine, and 54 lb of transducers, valves, and lines comprise the primary propulsion elements requiring structural support. A truss structure is provided which supports the two propellant tanks, and a ring assembly is furnished which surrounds the two propellant tanks in a horizontal plane, provides attach points for pressurant tank support struts, and provides mounting surfaces for the high-pressure nitrogen gas plumbing. The tops of the propellant tanks are joined together by a bridge-like "thrust plate" structure, which in turn supports the rocket engine and all fuel and oxidizer plumbing.

The thrust plate, the ring assembly, and the truss structure comprise the primary elements of the 26-lb propulsion support structure, and serve to support the 1300-lb propulsion subsystem. Each of the support structure's primary elements incorporates design features worthy of description.

b. Beryllium truss structure. The truss structure was originally envisioned as a traditional aluminum-tube aluminum-fitting riveted truss, utilizing swaged tubes of various wall thicknesses to minimize fitting size and tubing stress variations. Such a truss would have weighed approximately 18.25 lb. To reduce truss weight, an alternative design concept was selected, utilizing beryllium tubing adhesively bonded to magnesium fittings. All truss members used the same diameter and wall thickness of tubing, thereby reducing beryllium tubing procurement problems and producing a finished beryllium truss weight of 6.25 lb, about 0.5 lb more than optimum. Key design and fabrication decisions were made as follows:

(1) *Adhesively bonded joints.* Because of the notch sensitivity and limited plasticity of extruded beryllium tubing, classical riveted, bolted, and threaded joints are not attractive fabrication techniques for a beryllium truss structure. Distortion and processing problems also make welding essentially impossible and brazing very unattractive. Adhesive bonding was the joining technique selected.

Adhesive joint selection. In an attempt to minimize fabrication problems on the *Mariner* Mars 1971 propulsion support truss, room-temperature-curing Epon 913 was chosen as the adhesive. This paste adhesive was

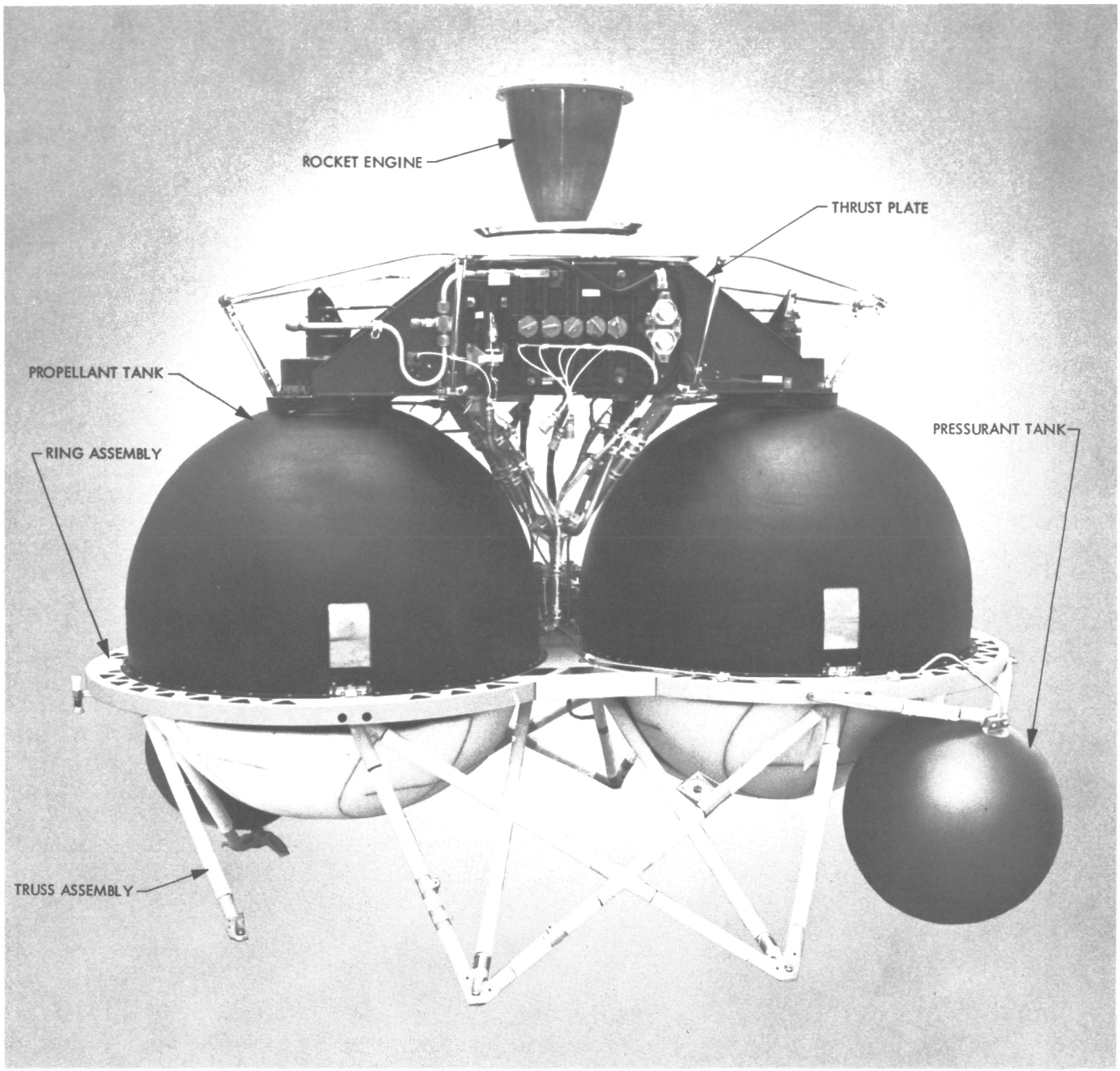

Fig. 4. Propulsion module

injected with a pneumatic (Semco) gun at 130 psi into a 2- to 10-mil annular gap formed between the beryllium tube and an externally concentric cylindrical magnesium fitting. Paste, rather than liquid, was chosen to eliminate the problem of adhesive draining out of the joint prior to curing.

(2) *Extruded beryllium tubing.* Beryllium extrusions are not yet so standardized that a particular shape may be chosen from a catalog then simply ordered with a specified heat treat and associated guaranteed properties. Instead, it is necessary to work closely with a vendor to reach, for a particular design, the best balance of dimensional accuracy, section thickness, strength, ductility, and cost. In the case of the *Mariner* Mars 1971 tubing procurement, the Nuclear Metals Division of the Whitaker Corporation produced very high-quality tubing with the following typical properties: tube compressive yield,

59,000 psi; tube compressive ultimate, 106,000 psi; tensile ultimate, 70,000 psi; outside diameter, 0.750 ± 0.008 in.; wall thickness, 0.040 ± 0.004 in.; straightness, 0.050 in 30 in.; and extrusion billet quality equivalent to Berylco HP-20 Type II. Only one minor tubing quality problem was encountered in the inspection of the *Mariner* Mars 1971 beryllium tubing, and that was the discovery of some approximately 5-mil-diameter 5-mil-deep surface pits on the as-received tubes. There was initially some concern that the pits would cause a reduction in tubing strength. Pull tests revealed, however, that all tubes gave ultimate tensile strengths in the range of 69- to 74-k psi, with no pitting-to-strength correlation evident. Further exploration revealed that the pits were formed during chemical milling of the tubes as a result of micro-contaminant removal by the chemical milling solutions. The pits were smoothly etched and round-bottomed with no evidence of any cracks radiating from them and were deemed non-deleterious to the beryllium tubing's structural quality.

Special handling precautions. Beryllium's most serious problem in structural applications is low toughness, i.e., low resistance to crack propagation. For reliable performance, it is necessary that *all* surface cracks be eliminated from a beryllium structural element. In practice, this is achieved by chemically milling 1 to 2 mils from the surfaces of a beryllium element after all machine work is completed. Mechanical surface removal as gentle as light buffing with 400 grit paper will initiate the micro-cracks which can precipitate failure. With this crack sensitivity in mind, the handling of the *Mariner* Mars 1971 beryllium tubing was planned to prevent surface abrasion during any part of the fabrication, testing, and launch operations. Surprisingly, it was quite easy to achieve abrasion-free handling of the tubes by the simple expedient of covering them at all times.

Beryllium toxicity. The *Mariner* Mars 1971 propulsion structure fabrication processes have been significantly influenced by consideration of beryllium toxicity. Beryllium tubing was bought cut to length to avoid cutting the tubing. Similarly, the chemical milling to eliminate surface cracks was done by the vendor even though subsequent shipping and handling then required special precautions to avoid surface abrasion. Lastly, the beryllium surface preparation for bonding was chosen largely due to the non-salt-producing nature of its chemistry. As a result of these simplifying steps, fabrication of the *Mariner* Mars 1971 propulsion structure was accomplished in a routine manner, with essentially no fabrication problems occurring as a result of using beryllium in the assembly.

(3) *Magnesium fittings.* To minimize weight, the *Mariner* Mars 1971 truss fittings were machined from ZK60A-T5 magnesium. Magnesium's low density minimizes the weight penalty of geometrically required unstressed material, and since the strength-to-weight ratio of ZK60A-T5 is about equal to that of 2024-T4 aluminum, no real weight penalty is imposed at highly loaded areas of the fittings.

(4) *Adhesive joint injection.* The joints were certified in the following manner: (1) Magnesium test fittings were Dow-17-coated and stored simultaneously with the coating of the flight fittings. These test fittings were then used in certification pull tests to destruction, thereby establishing confidence in the magnesium surface preparation. (2) Beryllium tube test specimens were conversion-coated simultaneously with the coating of each set of flight tubes. These test specimens were then bonded into test fittings with the same mix of adhesive used on the flight truss assemblies. The resulting test assemblies were pulled to destruction, thereby certifying the beryllium surface preparation and the adhesive quality. (3) The flight fittings were provided with four adhesive bleed holes, 90-deg apart, near the end of the inserted beryllium tube. Adhesive forced into the bond annulus at the top of the fitting (Figs. 5, 6, and 7) flowed the length of the tube-joint overlap, then bled out of the holes at the bottom of the fitting, at which time injection was stopped. Logic, destructive testing, and joint dissection all confirmed that this positive displacement adhesive injection technique reliably produced a completely filled bond annulus.

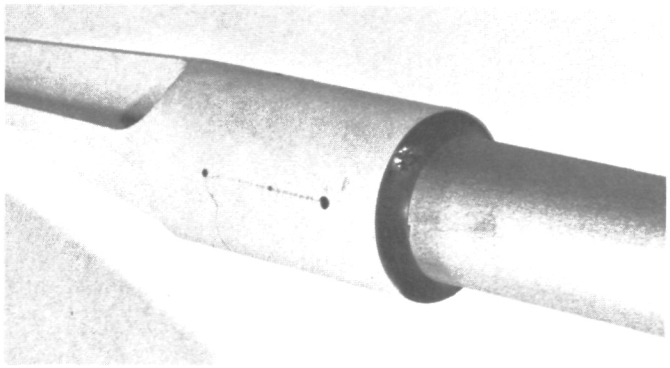

Fig. 5. Fitting bonded to beryllium tube

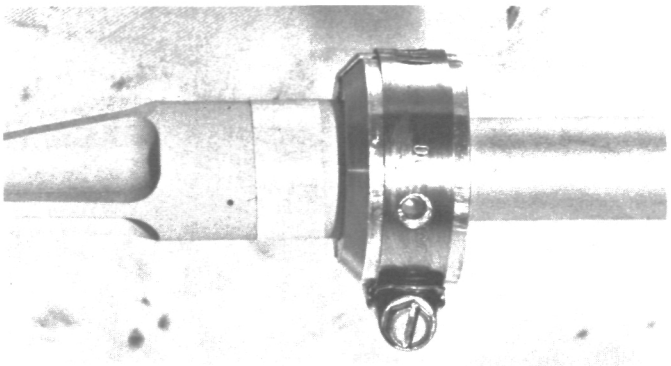

Fig. 6. Adhesive injector in place on fitting

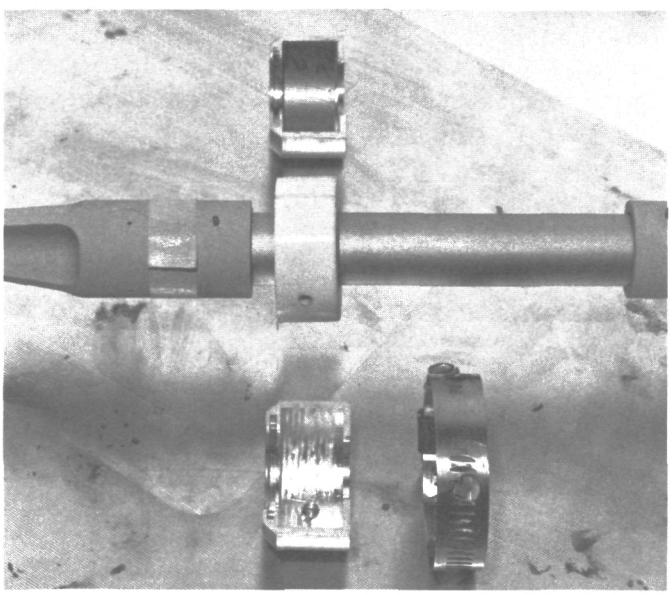

Fig. 7. Exploded view of tube fitting and injector

c. Thrust plate. The thrust plate (Fig. 8) is a large bridge-like structure which spans the 34-in. distance between propellant tanks and which supports the rocket engine, engine gimbaling actuators, fuel and oxidizer control valve assemblies and associated lines, filters, transducers, etc. To eliminate assembly tooling and tolerance build-up in manufacture of piece parts and to provide optimum structural paths without the excess weight of structural joints, each thrust plate was machined as one piece from a ZK60A-T5 magnesium forging. Typical wall thicknesses of 0.050 in. were maintained throughout, the surfaces of the plate being latticed with webs and bosses to provide attach points for propulsion components.

d. Ring assembly. The ring assembly (Fig. 9) is composed of two box section rings, 1.25-in. deep with approximately a 30-in. inside diameter and 36-in. outside diameter. The rings are joined together on one side by a large mounting plate assembly, and on the other side by a simple box beam.

The plate assembly is made up of two 50-mil-thick plates bolted back to back, each with $\frac{5}{8}$-in.-high webs and propulsion equipment mounting bosses integrally machined on both sides. Sandwiched between the plates are the two rings which surround the propellant tanks. Fabricated from ring-forged ZK60A-T5 magnesium billets, these rings were machined into a "C"-shaped cross section with 30-mil top and bottom panels and 60-mil ID and OD walls. The C section was then closed into a box section by blind (Huck) riveting a 20-mil magnesium cover plate onto the top panels. The inside diameter of the rings was held to a close tolerance (± 5 mil) to minimize fit problems with the propellant tanks, but this toler-

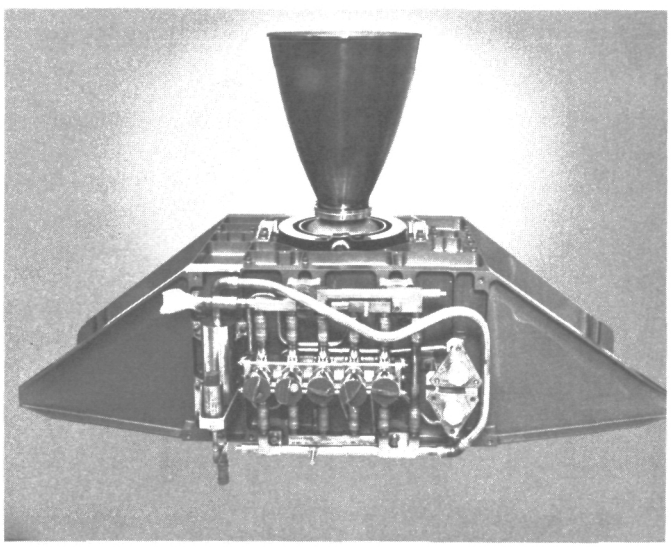

Fig. 8. Propulsion module thrust plate

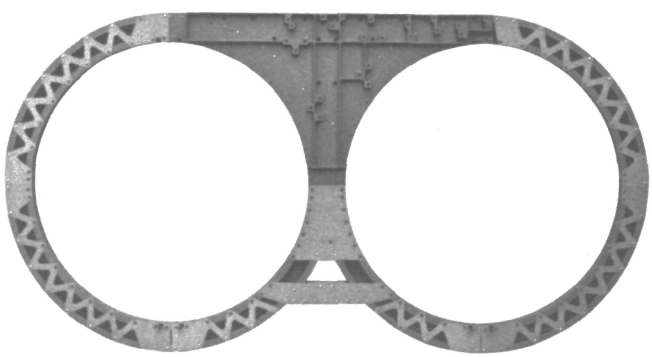

Fig. 9. Ring assembly, top view

ance proved not to be a problem due largely to the very stable nature of ZK60A-T5 material, and to the inherently small assembly stresses induced by blind riveting.

e. Conclusions. In summary, the propulsion support structure made extensive use of magnesium, most major structural elements being ZK60A-T5. This alloy demonstrated exceptional stability even when very large thin sections were machined from massive forgings. Blind riveting, even in non-blind applications, proved almost a necessity where close tolerances were to be maintained on large thin-walled riveted assemblies.

The surface preparation of beryllium structural elements was accomplished by conversion-coating the surface with Berylcoat-D. This surface preparation provided corrosion-resistant surfaces which could stand a reasonable length of time (24 h) between cleaning and bonding and not adversely affect bond strength. Further, the surface preparation produced no toxic beryllium salts or powder, and was, therefore, usable in a production shop without imposing costly time-consuming safety restrictions.

The uncommonly high *stiffness*-to-weight ratio of beryllium (seven times that of aluminum, magnesium, titanium, or steel) permitted a major weight savings in the truss structure. For the *Mariner* Mars 1971 spacecraft, 2.4 lb of beryllium tubing replace approximately 12.4 lb of aluminum tubing and provide increased structural rigidity. As a cautionary note, the *strength*-to-weight ratio of the *Mariner* Mars 1971 beryllium tubing is only about 50% better than that of very high-strength aluminum extrusions (such as 2024-T851); therefore, it is in the design of stiffness- (not strength-) controlled structures that beryllium's weight-saving potential may be fully realized.

Adhesively bonded joints proved to be the key for practical application of beryllium to a spacecraft structure. Careful attention to surface preparation and adhesive injection techniques resulted in consistently high-strength joints with no joint failures.

3. Flight Cabling

Design change accomplished on *Mariner* Mars 1971 required several significant modifications to the *Mariner* Mars 1969 flight cabling subsystem. The spacecraft cabling is depicted in Fig. 10. While all wiring harnesses were modified to accommodate detail changes in electronics assemblies, major redesign was required in Bays I, II, VIII, and the solar panel and pyro wiring harnesses.

The power subsystem harnesses were redesigned to accommodate changes required by the repackaging of power regulation from Bay VIII to Bay I and power conversion from Bay I to Bay II. The 2.4-kHz power interconnect cables now interface directly between Bays I and II, by-passing the upper ring power harness; and all power harnesses incorporate multiple redundant conductors to minimize voltage drop.

The pyro switching assembly was relocated from Bay I to the upper ring support structure, which required redesign of the pyro interconnect wiring harness. The redesign includes provisions for separation of the propulsion subsystem from the bus to permit separate testing.

The propulsion pyro wiring harness was designed to accommodate the new propulsion subsystem. The new harness provides for control of 15 propellant valves, as compared to 8 valves used on *Mariner* Mars 1969.

Redesign of the attitude control subsystem required redesign and rerouting of cables to acquisition sun sensors, sun gate, gas valves, and gimbal actuators.

New wiring harnesses were designed to accommodate the infrared interferometer spectrometer (IRIS), which replaced the infrared spectrometer.

The television subsystem wiring harness was revised to accommodate TV electronics changes, and the shielding techniques were revised to reduce interference conditions existent in *Mariner* Mars 1969.

The wiring harnesses from Bay II (scan and IRIS) and Bay VII (data automation subsystem and TV) to the science platform have grown approximately 10%, and now include high-voltage power for the IRIS.

The power ring umbilical harness incorporated additional stimulus lines for the ultraviolet subsystem, IRIS, and TV, and index pins were located on the separation connectors to assure proper mating with test cables.

4. Thermal Resistance at Chassis–Subchassis Interface

A thermal–vacuum joint conductance test was conducted to determine the following:

(1) Overall thermal resistances across standard 6- and 14-in. electronic subassembly/shear plate joints.

(2) Thermal resistance per mounting screw for electronic subassembly/shear plate joints.

(3) The effect of flange flatness on thermal resistance of the electronic subassembly/shear plate interface.

Three types of subassemblies were tested:

(1) Old standard *Mariner* Mars 1964 6-in. subassemblies with a standard three-screw pattern on the mounting flange.

(2) A standard *Mariner* Mars 1971 14-in. subassembly with a standard 5 screw pattern on the mounting flange.

(3) A standard *Mariner* Mars 1971 14-in. subassembly with two additional screws added to a standard 5 screw mounting pattern.

All test items were magnesium. The shear plate was treated with Dow 17 and the subassemblies were treated with Dow 7. The 6-in. subassemblies were mounted to the shear plate with three No. 6 machine screws. The 14-in. subassemblies were mounted with three No. 6 screws in the center section of the mounting flange and two No. 8 screws through the heavy tabs at the ends of the mounting flange. All screws were torqued to flight specifications, 18-in.-lb for No. 6 screws and 35 in.-lb for No. 8 screws.

Power was supplied to the subassemblies with resistors screwed to the electronics mounting surface. Each individual subassembly was covered with a ten-layer thermal shield of aluminized mylar to minimize radiative heat losses and interchange between subassemblies. Temperatures were measured with thermocouples attached to each side of the mounting surface (Figs. 11 and 12).

Various power levels were established on each module and the temperature gradients measured across the joints midway between bolt locations. On one subassembly, the gradients were also measured at the bolt locations. A second series of tests was conducted with one No. 6 screw removed from the 6-in. subassemblies and two No. 6 screws removed from the 14-in. subassemblies.

The test results are summarized:

(1) The joint thermal resistance for a standard 6-in. subassembly varied between 1.95 to 2.38°F/W for a standard 3 screw pattern and between 3.37 to 4.25°F/W for a 2 screw pattern.

(2) The joint thermal resistance for a standard 14-in. subassembly varied between 1.00 to 1.40°F/W for a standard 5 screw pattern and between 1.86 and 2.6°F/W for a 3 screw pattern.

(3) The thermal resistance measured at the No. 6 screw locations varied from 2.31°F/W-bolt to 4.90°F/W-bolt. The average thermal resistance was 4.02°F/W-bolt.

(4) The data indicates that flatness of the mounting flange in the short dimension had negligible effect on thermal resistance in comparison with the removal of mounting screws from the subassembly.

5. DTM Static Test

a. Introduction. Early in the *Mariner* Mars 1971 program, it became evident that confidence in the load-carrying structure was going to require demonstration of limit load criteria. The addition of approximately 1200 lb of propulsion subsystem to the existing *Mariner* Mars 1969 design was going to result in a more marginal situation than in earlier *Mariner* programs, particularly for the bus, separation joint, and adapter. In addition, the basic structure of the propulsion subsystem, beryllium tubing with bonded magnesium fittings, represented a departure from construction techniques used in earlier programs and it also required demonstrated adequacy.

Forced response analysis indicated that design limit loading criteria[1] might be exceeded during system-level low-frequency forced vibration testing in the lateral axes. To assure that this critical loading could be adequately monitored during forced vibration testing, it was necessary to convert a portion of the developmental test model (DTM) adapter structure into a "load cell." Calibration of this "load cell" during static test was accomplished with a known bending moment, resulting from a lateral shear load at the spacecraft CG.

The following objectives were established for the *Mariner* Mars 1971 DTM static test program:

(1) Calibrate the strain gage instrumentation on the *Mariner* Mars 1971 adapter.

(2) Verify the structural integrity of the tank/tab attachment area and the beryllium truss feet/octagon interface.

[1]M71-3-190, *Mariner Mars Structural Design Criteria*, specifies a limit condition at the spacecraft field joint of 9,000 lb shear and a moment of 450,000 in.-lb.

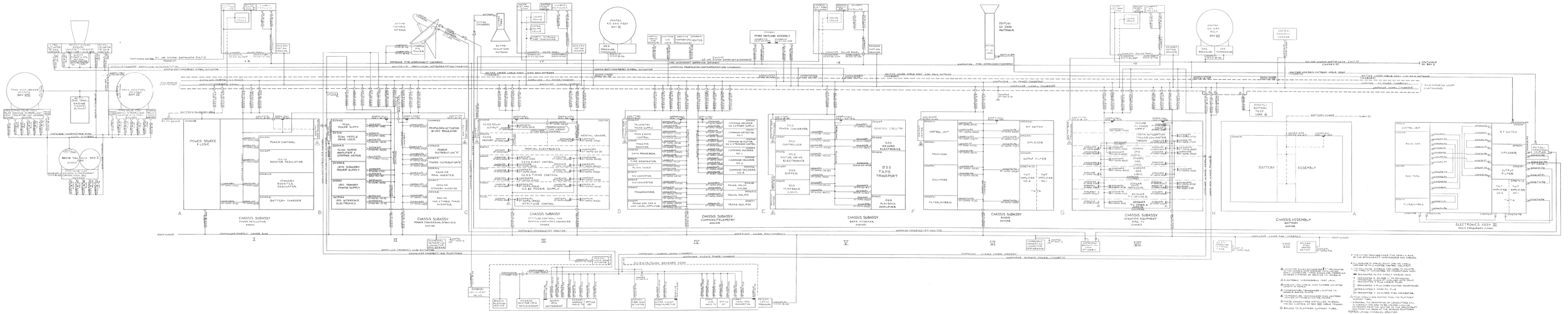

Fig. 10. *Spacecraft cabling block diagram*

Page intentionally left blank

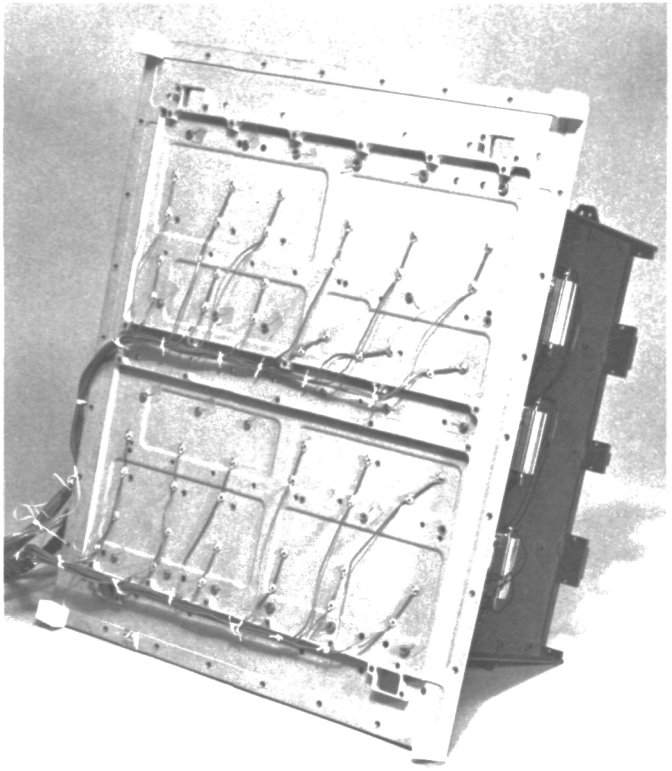

Fig. 11. Shear plate thermocouple installation

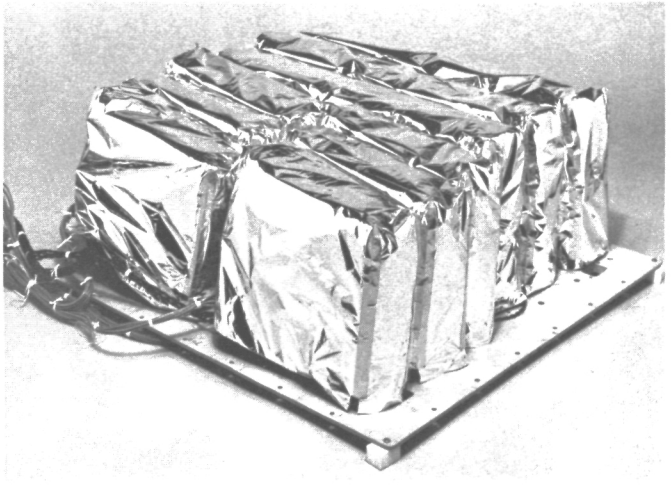

Fig. 12. Chassis thermal resistance test configuration

(3) Obtain static load distribution from the propellant tanks to the spacecraft adapter for comparison with the *Mariner* Mars 1971 analytical predictions.

(4) Investigate special conditions, such as the effects of propellant tank pressure on the stiffness of the propulsion support structure.

(5) Verify the structural integrity of the octagon, separation joint, and adapter when subjected to design limit load.

b. Description of testing. Test loads were applied to the DTM in two different configurations. Configuration 1 consisted of the lateral pull-test fixture, octagon structure, and *Mariner* Mars 1971 adapter mounted on the *Centaur* adapter (Fig. 13). The *Centaur* adapter was hard-mounted to the structural test floor. The pull-test fixture was designed so that a lateral load of 9,000 lb[2] could be applied through a plane passing through the spacecraft CG, which was located 10.0 in. above the top ring of the octagon. To determine the uniformity of adapter strain, the load was applied twice in directions 90 deg apart, as shown in Fig. 13.

Configuration 2 consisted of the same basic build-up of adapters and octagon as configuration 1. The pull-test fixture was replaced with a flight-quality beryllium truss and propellant tank assembly (Fig. 14). Referee fluids (Freon TF for the oxidizer and isopropyl alcohol for the fuel) were used to completely fill the propellant tanks. Loading was applied through the fuel tank by means of bonded shear straps attached to the girth of the propellant tank. Loading of the shear straps was accomplished with a hydraulic ram/whiffletree arrangement. The maximum load of 3,000 lb was applied to the propulsion subsystem in 10% increments, while the tanks were pressurized to 100 psig. To investigate the possibility of stiffness changes, lesser load levels were applied while the tanks were pressurized to 50, 25, and 10 psig.

c. Instrumentation and data reduction. The instrumentation for configuration 1 consisted of ten dial gages and eight sets of strain gages. The dial gages were located around various parts of the structure and visually moni-

[2]The 9,000 lb was derived from M71-3-190.

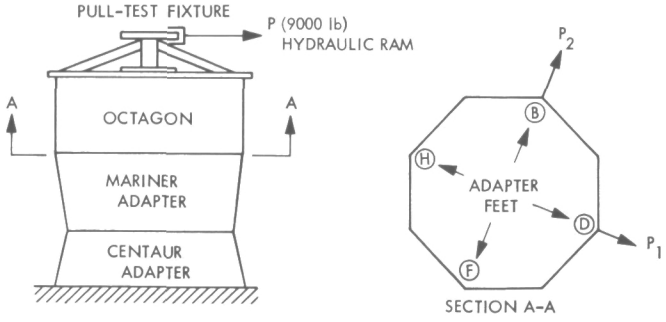

Fig. 13. Static test configuration 1 setup

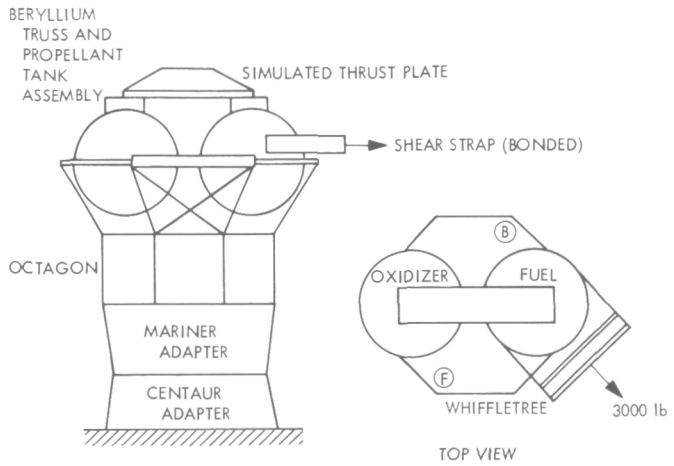

Fig. 14. Static test configuration 2 setup

tored to check anomalies, linearity, etc. The strain gage sets were located on each of the eight vertical longerons of the *Mariner* adapter. Strains were recorded on an automatic Datex system with printed and punched paper tape.

Instrumentation for configuration 2 consisted mainly of strain gages. Each of the four tabs of *both* propellant tanks was fitted with an axial strain gage. In addition, sixteen of the beryllium tubes in the support truss were instrumented with axial strain gages. Recording and data reduction were similar to those for configuration 1.

d. Results. A typical example of adapter strain, as measured from Configuration 1 testing, is shown in Fig. 15. These measured strains proved to be repeatable, linear, and uniform, with little evidence of hysteresis.

The resultant plots of the measured truss strains for configuration 2 are shown in Fig. 16. These plots proved to be highly repeatable and compared well with analytical predictions.

e. Conclusions. DTM static test conclusions are:

(1) The *Mariner* Mars 1971 adapter was accurately calibrated for use as a "load cell" for the DTM forced vibration test.

(2) The structural integrity of the tank/tab and truss foot/octagon interfaces was demonstrated.

(3) The measured values of truss strain showed good correlation with analytical predictions.

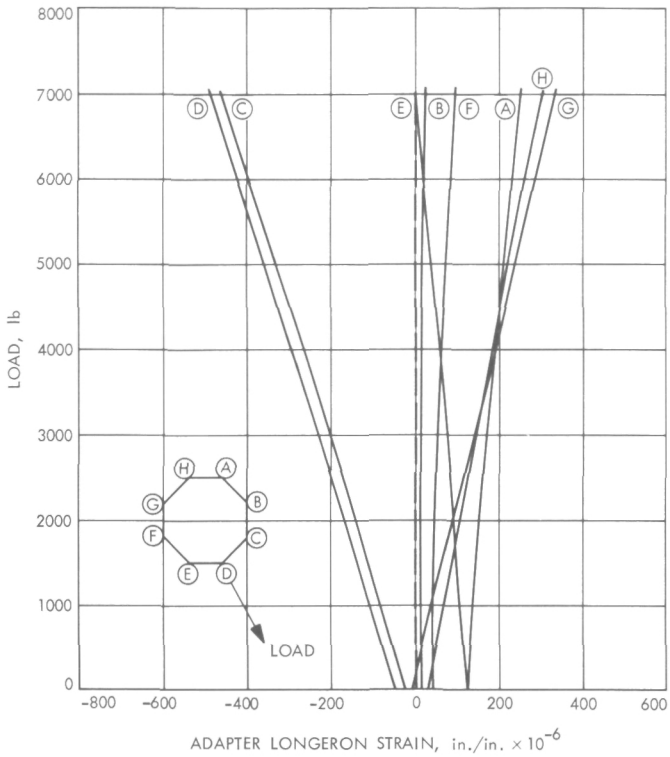

Fig. 15. Adapter strain vs load

(4) No changes in stiffness due to varying propellant tank pressures from 10 to 100 psig were detectable.

(5) The structural integrity of the DTM octagon, separation joint, and adapter were verified for exposure to design limit load.

6. Spacecraft Modal Survey

a. Introduction. A modal survey has been performed on the *Mariner* Mars 1971 DTM to obtain a dynamic normal mode mathematical model of the spacecraft and correlate this model with an eigenvalue solution obtained from a spring mass model. These models are used to determine the loads for the forced vibration test and the flight conditions.

b. Description of the survey. The spacecraft, except for solar panels and high-gain antenna, was cantilevered on the floor at the *Centaur* adapter level (Fig. 17).

The structure was excited with a maximum of eight 25-lb shakers, and the mode shapes were measured for each identifiable mode. The corresponding mode shapes were measured at 189 stations, representing 189 degrees of freedom. These measurements were made point by

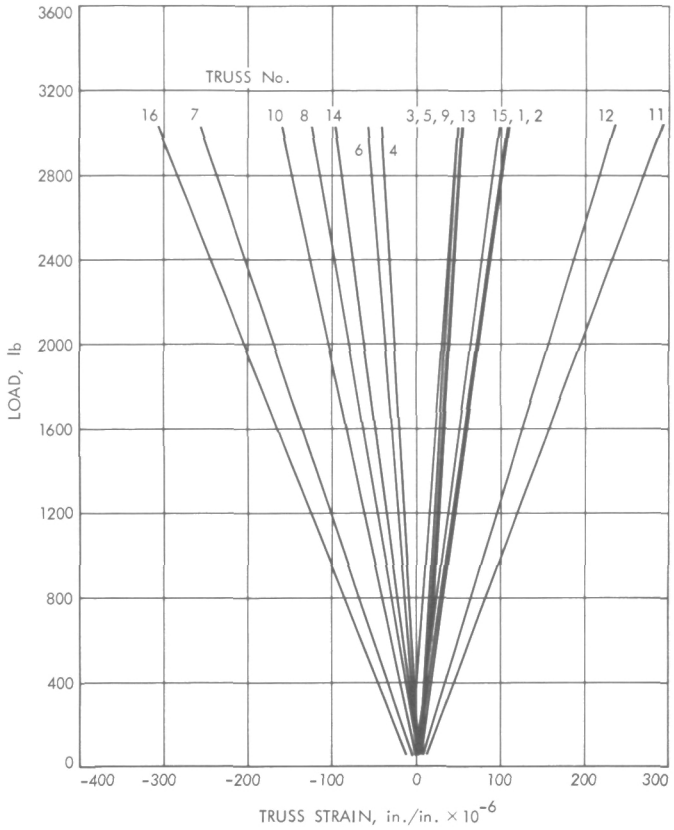

Fig. 16. Truss strain vs load

point with a rover accelerometer. The reading of the rover was compared to the reading of a reference accelerometer placed at a fixed location on the spacecraft. The amplitude ratio and phase of the angle between the rover and the reference were recorded for all rover locations.

The survey was made for two configurations:

(1) Case 1 where the tanks were completely full.

(2) Case 2 where ullages existed in tanks (5% for the fuel tank, 10% for the oxidizer tank).

The major differences between the full tank modes and the ullage modes were a marked frequency shift in the first two bending modes. This indicates a fuel mass relief due to the slosh modes and in the damping, which is up to 300% higher for the ullage condition than for the full tank condition. The amount of mass relief was determined by an independent tank test, from which it was found that not all the fluid mass was effective but that 80 lb should be subtracted for the fuel tank and 200 lb for the oxidizer tank.

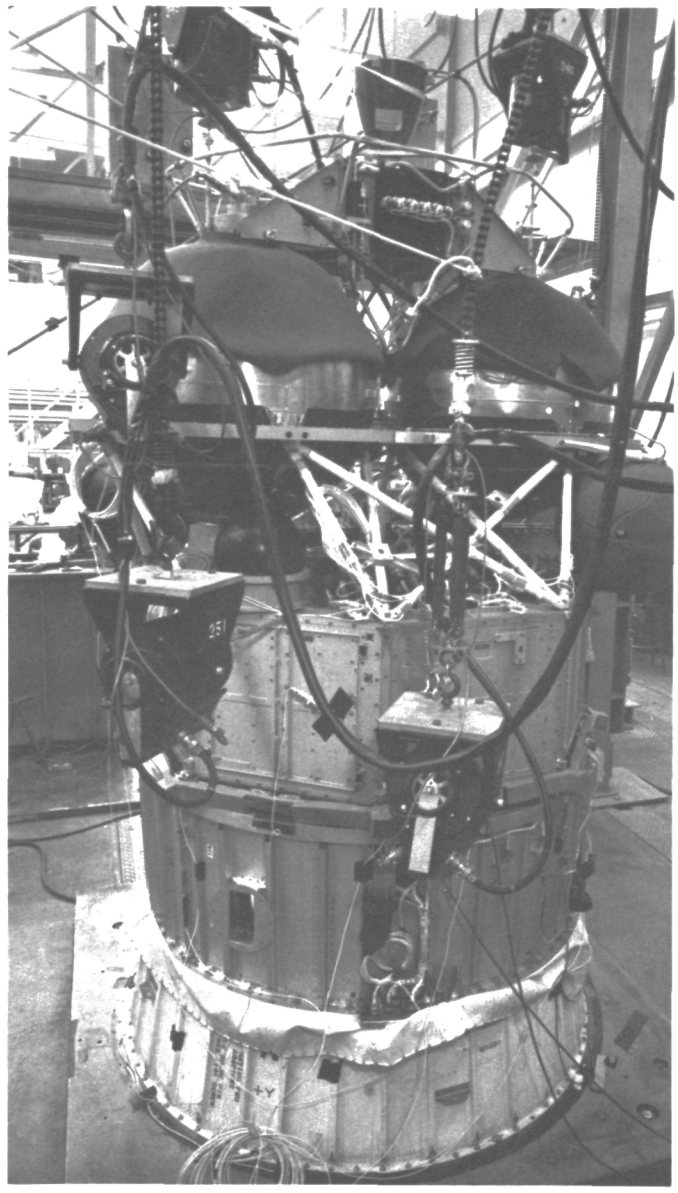

Fig. 17. Developmental test model modal test setup

7. Spacecraft Overturning Moment for Longitudinal Low-Frequency Environmental Vibration Test

a. Introduction. Because of a difference of weight between the fuel tank and the oxidizer tank, the *Mariner* Mars 1971 DTM spacecraft has a center-of-gravity offset of about 2 in. from the longitudinal or thrust axis. As a result, it was anticipated that an overturning moment of substantial magnitude could occur during the low-frequency system-level environmental vibration test in the z-axis configuration. A large overturning moment could have led to damaging effects on the armature of the shaker and possibly subsequent damage to the spacecraft.

Therefore, a detailed study and analysis of the problem was made to calculate the armature displacements during a simulation of the low-frequency vibration test.

b. Results. The modulus of the rotations and translations of the armature with respect to the shaker body (field) were computed for a frequency range from 1 to 200 Hz. The most severe response has been found to be about the y-axis perpendicular to the trunnion axis. A peak rotation of 0.13 rad/s^2 occurs at about 3 Hz. Since the allowable rotation of the armature was estimated to be 0.2 rad/s^2 and the test was not to start before 5 Hz, it was concluded that the overturning moment problem was not critical. Because of possible uncertainties in the data, the following step was taken.

An offset weight of 210 lb was bolted on the side of the fixture to bring the center of gravity back on the z-axis. The results of a rerun analysis show a drastic reduction of rotation in the frequency range of 1 to 15 Hz. The effect of the offset balance weight becomes ineffective above that range because of the elastic effect of the spacecraft. This offset weight was removed for the high-frequency tests, which started at 120 Hz.

8. Metallurgical Study of Burst-Tested Propellant Vessel

Details of the design utilized in construction of the *Mariner* Mars 1971 propellant vessel for containing MMH or N_2O_4 were reviewed in SPS 37-60, Vol. I, pp. 24–28. The first vessel constructed for this program (S/N 001) was designated as the burst test unit, after successfully passing a liquid-nitrogen proof test at 840 psig. The burst test was planned to provide data on local and bulk yielding, as well as to determine burst pressure and an opportunity for metallurgical characterization of microstructure, weld quality, and chemistry. The particular vessel tested exhibited excessive weld mismatch but still survived the 840-psig internal pressure applied during liquid-nitrogen proof testing.

This propellant vessel is a spherical unit fabricated from two titanium alloy (Ti-6Al-4V) hemispherical forgings which are machined and subsequently joined by TIG[3] fusion welding of a "burn down" joint configuration. The vessel is 29.5 in. in diameter, and has a 7.0-in. internal diameter port on one end and a small (1.87-in. diameter) pressurant port at the opposite end. Prior to the burst test, six strain gages were mounted to the vessel so that strain versus pressure data was available for areas of maximum predicted discontinuity stresses.

The burst test vessel was filled with distilled, deionized water at 78°F and installed in the pressure test apparatus. Closed-circuit TV/video-tape monitoring of volume change versus pressure was utilized during hydrostatic pressure build-up until rupture occurred. A video-tape record of the actual rupture appearance and propagation was also available. Pressure versus change in volume data was obtained (Table 3). Plotting this data and correlation with strain gage measurements indicate a bulk yield pressure of between 630 and 660 psig. Using thin wall membrane stress analysis, the burst stress was calculated to be 165,100 psi.

Examination of the burst test fragments revealed that the unit ruptured in a ductile manner. The deviations from original contour, together with the volumetric expansion data, substantiated the fact that normally expected large plastic deformation occurred during pressurization. The fracture initiated in the membrane portion of the pressurant port hemisphere approximately 4.5 in. from the polar axis (Fig. 18).

The fracture propagated from this area toward and across the girth weld into the upper hemisphere, causing the unit to nearly separate into two pieces. The original wall thickness in the fracture initiation region was 0.036 in. and was reduced to 0.031 in. upon rupture. A secondary failure was observed on the video tape when the transition tube extending from the pressurant port was broken off by contact with the tank support fixture as the unit was propelled upward by the water jet expelled from the rupture at the bottom of the test unit.

Table 3. Pressure vs change in volume data

Pressure, psig	Change in volume, ml	Pressure, psig	Change in volume, ml	Pressure, psig	Change in volume, ml
0	0	450	2665	725	4365
50	460	500	2941	750	4989
100	735	550	3210	760	5416
150	1018	575	3350	770	5711
200	1293	600	3479	780	6453
300	1838	650	3755	795	8422
350	2114	675	3906	800	8862
400	2380	700	4103	806[a]	9276

[a]Unit ruptured at 806 psig.

[3]TIG = tungsten inert gas.

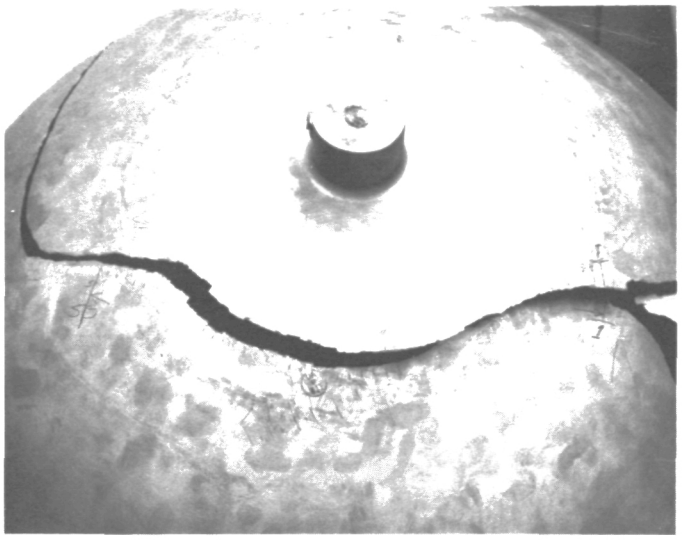

Fig. 18. Burst test vessel showing area of fracture initiation

A metallurgical examination of the test unit was conducted in the following steps:

(1) Microstructure characterization in membrane and boss areas.

(2) Microstructure of girth and tab welds.

(3) Microhardness variations across a weld.

(4) Microstructure of stainless steel-to-titanium transition tube joint.

(5) Hydrogen analysis of membrane and weld areas.

Results of each step are illustrated by Figs. 19–22.

Several conclusions can be made upon review of the results:

(1) The fracture initiated within an area of large discontinuity stresses at a pressure expected from earlier stress analysis.

(2) Plastic distortion prior to failure and a microstructure with 30% or more primary alpha phase in an alpha–beta matrix indicate that the vessels should exhibit acceptable toughness in actual use.

(3) Hydrogen in the membrane and weld areas was well below the 125 ppm maximum allowed to minimize embrittling effects.

(4) A large girth weld mismatch in excess of the 0.010-in. maximum specification allowed did not deter the vessel from performing in an acceptable manner.

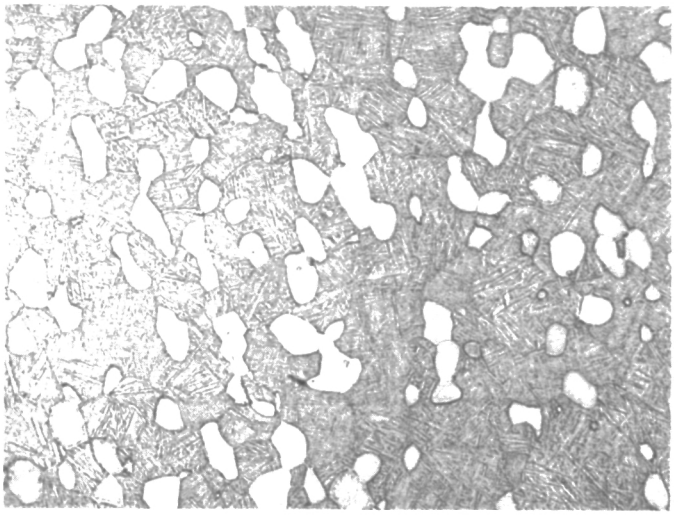

Fig. 19. Typical boss area microstructure, showing distribution of constituents associated with adequate toughness

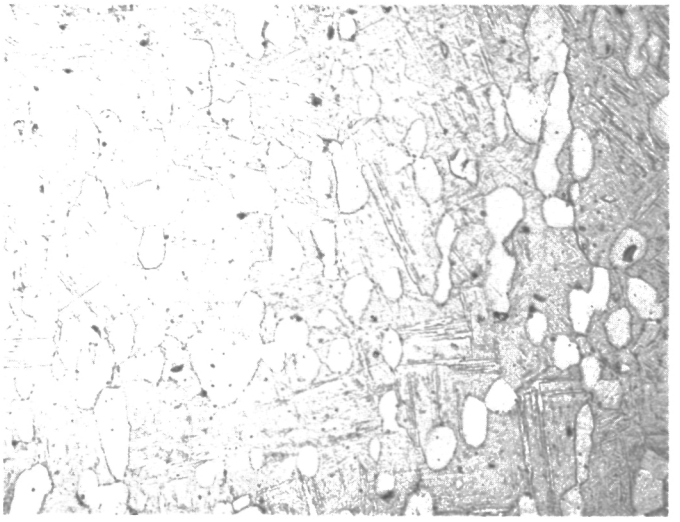

Fig. 20. Typical membrane area microstructure, showing distribution of constituents associated with adequate toughness

9. Electronic Parts Control

a. Background. Parts control at JPL describes the technical discipline whose responsibility it is to assure the use of the best available electronic/electromechanical parts, properly applied and 100% screened. This process starts long before circuit design and continues through the life of the spacecraft program. Parts control encompasses several activities:

(1) Parts qualification/evaluation.

(2) Parts selection.

Fig. 21. (a) Typical girth weld microstructure/microhardness (DPH) 375 to 405; (b) girth weld microstructure in area of worst mismatch

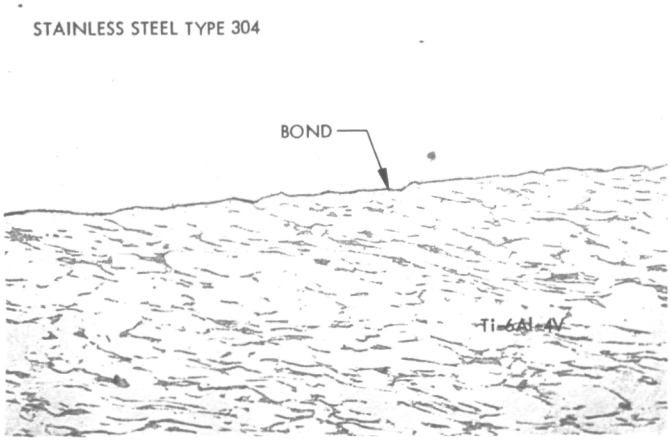

Fig. 22. Typical microstructure of transition tube bond between type 304 stainless steel and Ti-6Al-4V produced by co-extrusion, showing desirable narrow metallurgical bond line

(3) Specification writing and review.

(4) Parts screening.

(5) Application review and design appraisal.

(6) Failure analysis.

(7) Parts listing.

The Electronic Parts Engineering Section has been applying a concentrated effort from program to program over the past several years to enhance the reliability of electronic/electromechanical parts through the improvement of each of these seven activities. The following paragraphs describe the *Mariner* Mars 1971 parts listing activities.

b. Parts listing activities. The *Mariner* Mars 1971 Electronic/Electromechanical Parts Design Control List (610-12) is composed of individual subsystem parts lists and a composite spacecraft parts list.

(1) *Necessary inputs.*

Preliminary parts lists. The preliminary parts lists must be transmitted to the JPL part specialists for their review and approval. These lists may take any form convenient to the subsystem contractor or JPL cognizant engineer, but must contain the following information:

(a) *Part number.* Manufacturer's part number and subsystem contractor's part number, if one is assigned.

(b) *Part manufacturer.*

(c) *Applicable specification.* All applicable procurement and screening specifications must be identified. If the part is purchased to a manufacturer's in-house specification rather than a JPL or system contractor's specification, it should likewise be identified.

(d) *Quantity used per subsystem per spacecraft.*

Specifications. All applicable procurement and screening specifications must be transmitted to the JPL parts specialists for their review and approval.

Application. On all new and modified design, parts stress analyses are to be performed by the design agency and transmitted to the JPL parts specialists for their review and approval.

(2) *Classification.* Classification is here defined as a composite rating of the three main elements of each line item of the Parts Control Summary List:

(a) Part number/part manufacturer.

(b) Procurement and/or screening specifications.

(c) Application (as identified by parts stress analyses).

The JPL parts specialists are responsible for rating each of the three elements mentioned above. Having rated each element, the final classification of the combination of the three may be found by referring to Table 4.

Table 4. Classification of elements

Element	Classification			
	1	2	3	4[a]
Part number/part manufacturer	Q	A	T	By/Bx
Procurement/screening specification	A	A	A	U
Application	A	A	A	U

[a]If any one of the three elements is unacceptable (By, Bx, or U), the resultant classification is 4.

The following describes the basis for rating each element.

Part number/part manufacturer. The first element may be rated acceptable, in test, or unacceptable:

Acceptable	
Q	On the current issue of the JPL Preferred Parts List; formally qualified by JPL Electronics Parts Engineering Section or subcontractors' qualification test results reviewed by the Electronics Parts Engineering Section and found to be acceptable.
A	Only limited qualification/evaluation performed; adequate for *Mariner* Mars 1971 use; may or may not be further qualified.
In test	
T	Part (or part family) is on test or scheduled for test during current fiscal year.
Unacceptable	
By	Not recommended for spacecraft use based upon lack of adequate reliability data or indication from available history that part, while not catastrophic, has certain characteristics which make it less than desirable.
Bx	Found to be inferior and definitely not recommended for spacecraft use. Use of the part presents serious risk to spacecraft.

Procurement/screening specifications. The second element may be rated acceptable or unacceptable:

A	Acceptable; meets JPL minimum requirements.
U	Unacceptable; does not meet all of JPL Electronics Parts Engineering Section screening requirements.

Application. The third element, likewise, may be rated acceptable or unacceptable:

A	Review of parts stress analyses shows part is adequately derated and properly applied.
U	Review of stress analyses shows part to be improperly applied or derated.

(3) *Assembly and updating of Parts Control Summary List.* To generate the list, accurate, timely inputs are necessary. These inputs (viz., preliminary parts lists, controlling specifications, and stress analyses) should be transmitted by the subsystem contractor through the appropriate cognizant engineer to the designated Electronics Parts Engineering Section parts representative, and from the parts representative to the Parts Engineering Group. Important, also, is the timely transmittal of updated information and specification revisions.

(4) *Status of parts listing.* The first issue of the *Mariner* Mars 1971 Electronic/Electromechanical Parts Design Control List (610-12) has been released. An updated list is being compiled.

D. Propulsion

1. Propulsion Subsystem

a. Description. Previous *Mariner* spacecraft employed small monopropellant propulsion systems to accomplish one or two trajectory correction maneuvers prior to planetary flyby. For the *Mariner* Mars 1971 spacecraft, it was necessary to evolve a new large bipropellant system to accomplish (1) in-transit trajectory correction maneuvers, (2) deceleration of the spacecraft into orbit about Mars, and (3) adjustments to the orbit as required.

Figure 23 is a schematic diagram of the propulsion subsystem. The subsystem is functionally a regulated-pressure, constant-thrust bipropellant propulsion system employing (1) gaseous nitrogen pressurant stored at 3650 psia within two 15-in.-diameter titanium vessels, (2) teflon-bladdered, 30-in.-diameter propellant tanks capable of storing approximately 1000 lbm of propellants, (3) explosively actuated isolation valves in both the pressurant and liquid circuits, and (4) a 300-lbf-thrust conduction-cooled rocket engine. The subsystem consists of nine major subassemblies, shown by dotted lines on Fig. 23. A major subassembly consists of a group of components that can be physically located together and that can be tested as a unit.

Figure 24 is a photograph of the subsystem. The propulsion module is designed to be an entity, with truss members and ring sections structurally supporting the tanks, pressure vessels, and associated valving. The module structure is integrated with a bridge box section between tanks to support the engine, gimbals, and related plumbing. Table 5 outlines the key subsystem characteristics.

Table 5. Propulsion subsystem characteristics

Parameter	Value or type
Engine thrust, lbf	300
Fuel	Monomethyl hydrazine
Oxidizer	Nitrogen tetroxide
Flow rate, lbm/s	1.06
Oxidizer/fuel ratio	1.55
Propellant capacity, lbm	1020
Specific impulse, lbf-s/lbm	283

The propulsion subsystem design has been completed, most subassemblies have been fabricated, and the first complete module, designated the engineering test model, has been assembled. Two aspects of the program are discussed: (1) the results of some development system model (breadboard) tests at Edwards Test Station, and (2) a description of a digital computer program developed to support the flight operations.

b. Development system model tests. A series of three tests was conducted on a development system model (DSM) propulsion system to evaluate the general operation and characteristics of the *Mariner* Mars 1971 propulsion subsystem. This breadboard system contained the essential elements of the flight subsystem, although several components utilized were similar in design, but not identical to flight configuration. The tests were conducted under ambient conditions, rather than in a vacuum condition.

The results observed during the DSM tests indicated the need for redesign of certain elements of the flight propulsion subsystem, indicated the need for further evaluation in certain areas, as well as indicating confidence in performance and operation in other areas.

The items that were redesigned were:

(1) The ¼-in.-diameter low-pressure gas system tubing, between the regulator and the propellant tanks, was replaced by ⅜-in.-diameter tubing to prevent overpressurization at the regulator outlet during pyro valve opening transients.

(2) A by-pass connection in the gas side of the propellant tanks was designed to allow tank venting in the launch position.

(3) The flex lines were pre-formed to reduce side loads on the actuator to acceptable levels.

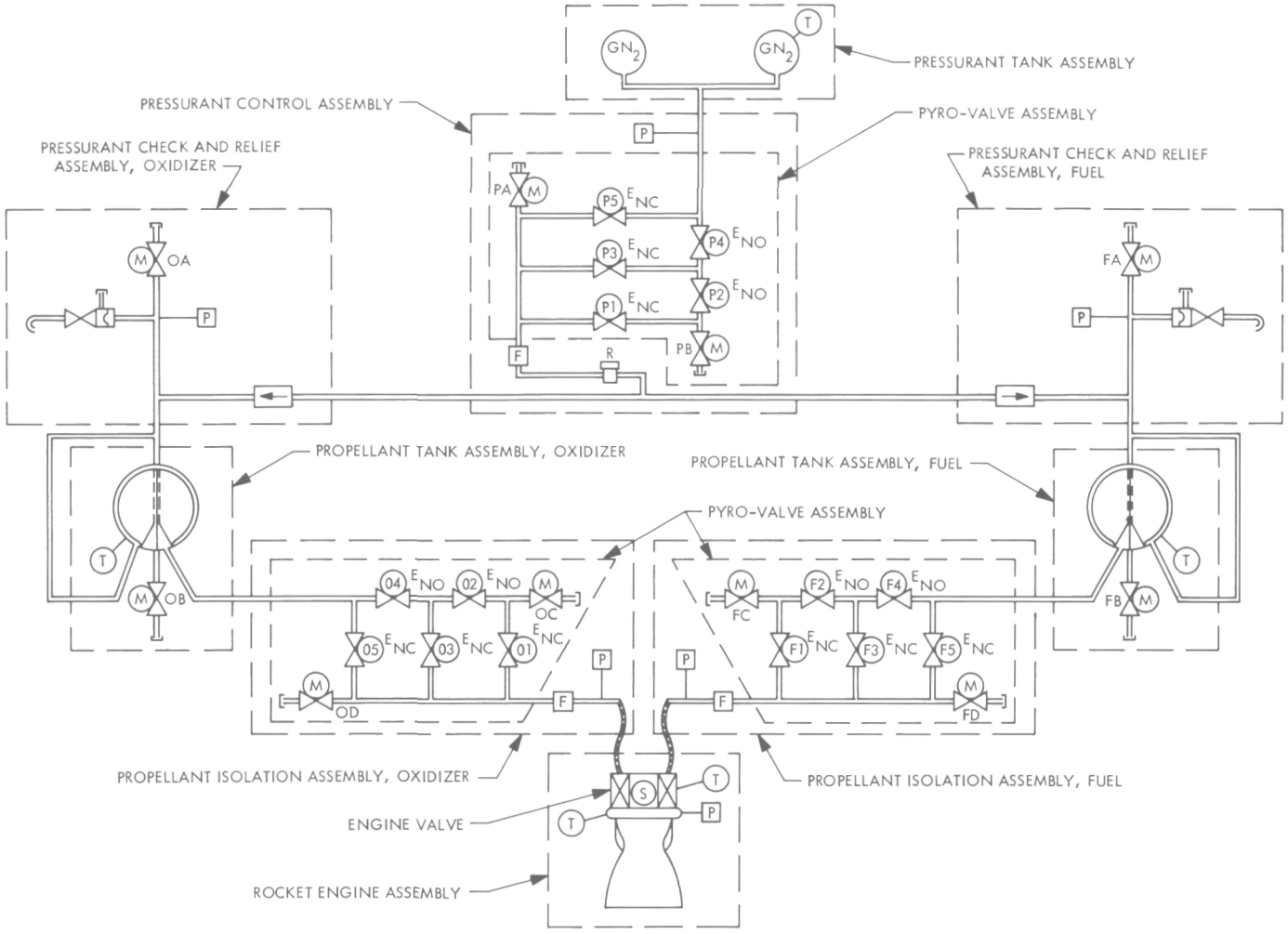

Fig. 23. *Mariner* Mars 1971 subsystem

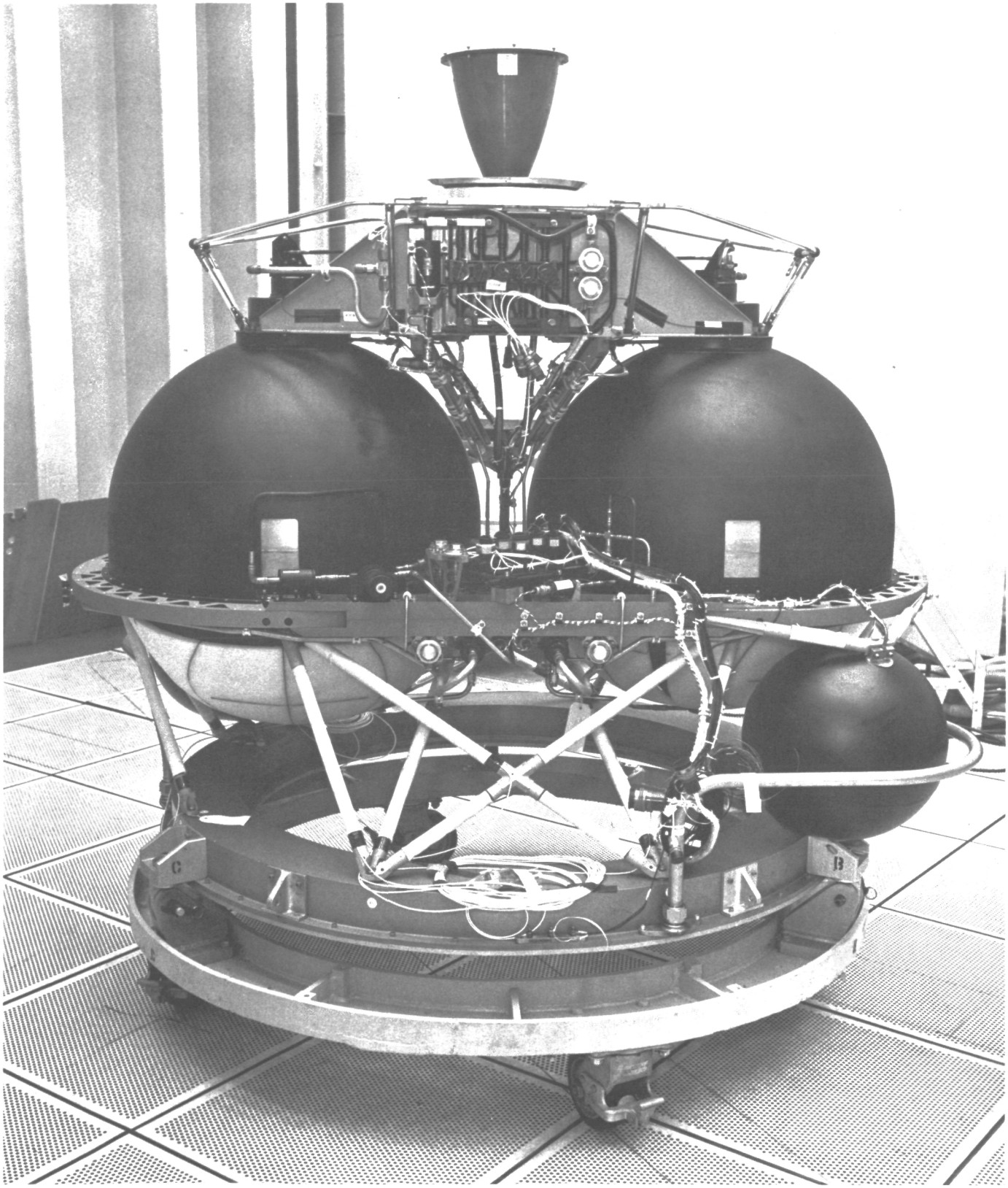

Fig. 24. Propulsion subsystem module

The items that needed further evaluation were:

(1) Saturated oxidizer causes an outgassing condition during pyro valve opening transients, which alters the engine start transient characteristic. Further evaluation is required to establish repeatability of the start transients.

(2) Feed-line pressure surges, during pyro valve opening transients and engine shutdown transients, were significantly higher than predicted. Further evaluation of the structural integrity of feed system components, specifically the standpipe and pressure transducer, was indicated.

The items that indicated confidence in performance and operation were:

(1) The subsystem performed near predicted values with respect to mixture ratio and thrust.

(2) Propellant was loaded and unloaded satisfactorily.

(3) The regulator controlled tank pressures satisfactorily during firings.

(4) The engine started, ran, and shut down satisfactorily when mated with the feed system.

(5) Activation, instrumentation, and procedures to be utilized for later testing on the engineering test model and type approval subsystems were utilized and satisfactory experience was achieved.

(6) Nitrogen-saturated oxidizer caused the same level of mixture ratio shift that has been experienced on engine level tests.

c. Operation and performance computer program. A digital computer program called Propulsion Subsystem Operation and Performance (PSOP) is being developed to support *Mariner* Mars 1971 flight analyses. PSOP is a low-frequency simulation model of the complete propulsion subsystem and will predict system pressures, temperatures, propellant and pressurant flowrates, thrust, spacecraft weight distribution, spacecraft acceleration, total velocity change, thrust pointing angles, and gimbal actuator lengths. The program will be used to predict flight telemetry data, generate thrust and spacecraft-mass time functions for flight maneuver analyses, perform malfunction analyses, and investigate effects of variations in system initial conditions.

A discussion of PSOP can be conveniently subdivided into two areas. The first area involves the flow of fluids within the subsystem and yields the common propulsion system pressure and temperature performance parameters. The second area involves the spacecraft mass and mass distribution, and yields the thrust pointing angle, total velocity increment, and gimbal actuator positions.

Propulsion subsystem performance. The propulsion subsystem contains the following major components: gaseous nitrogen pressurant tanks, gaseous nitrogen pressure regulator, fuel propellant tank, oxidizer propellant tank, rocket engine, and propellant lines and valves. The model was formulated by first describing the significant physical processes in each of the components and then organizing these descriptions into a large equation set. Like the physical hardware, component identity has been retained and interactions between components (equations) is required to achieve a system solution.

In general, the significant physical processes include heat transfer, gaseous compression and expansion, gaseous release from saturated propellants, pressure regulation, fluid flow, distributed hydraulic resistance, and chemical combustion. Heat transfer concerns both external radiation and internal convection. External radiation heating is considered for the nitrogen pressurant tanks, pressure regulator, and propellant tanks.

Internal convective heat transfer is described between the nitrogen pressurant tank and the enclosed gas, and between the pressurant in each propellant tank and the surrounding tank enclosure and liquid propellant. The gas in the pressurant tank and the gas in the propellant tanks may compress or expand according to real gas thermodynamic functions. Energy and mass balances are maintained in each tank to determine the state of the gas and the mass of both gas and liquid in each container.

The pressure regulator description is based upon real regulator characteristics and allows the regulated pressure to vary as a function of flowrate and inlet pressure. Each propellant tank is treated independently and pressurant flow is allowed only when the ullage pressure is lower than the regulator outlet pressure.

The amount of nitrogen gas absorbed by the propellants can be specified as a saturation level. If the level is sufficiently high, the gas will come out of solution in the liquid feed lines and cause a hydraulic resistance increase at the injector. Such an increase produces shifts in mixture ratio, chamber pressure, and engine thrust.

Engine chamber pressure and thrust are based upon instantaneous propellant flowrates and chamber geometry. The characteristic exhaust velocity, combustion

efficiency, and throat area are all variables with the characteristic exhaust velocity being a function of chamber pressure and mixture ratio. The throat area and combustion efficiency are empirically derived time functions and reflect the thermal changes in the thrust chamber hardware.

Spacecraft mass distribution. The propulsion performance portion of PSOP keeps track of the varying mass elements of the spacecraft, i.e., the instantaneous mass of oxidizer, fuel, and gaseous nitrogen in the various containers. This information is coupled with the fixed spacecraft mass in an eight-element mass model to determine total mass and spacecraft center-of-gravity location.

Since the guidance and control system forces the thrust vector to point through the spacecraft center-of-gravity, the thrust pointing angle can be determined from the location of the center-of-gravity and the engine gimbal center. The engine gimbal center will shift during long engine burns due to thermal growths in the hardware. This shift is described by a function of burn time and is based in part upon empirical measurements.

The gimbal actuator positions are computed from the thrust pointing angle and the results are converted to telemetry voltages. The motivation for modeling the gimbal system in PSOP comes from the desire to obtain information which can infer an engine burn mixture ratio. Since the spacecraft center-of-gravity movement during a burn is a measure of the integrated engine mixture ratio, and the gimbal actuator arm lengths indicate the direction of the spacecraft center-of-gravity, average engine mixture ratio can be inferred from the gimbal actuator positions.

General capabilities. PSOP will simulate pre-burn, burn, and post-burn behavior. During pre- and post-burn phases, the dominant processes are low-rate heat transfers. Thus, after a long burn when the gas in the propellant tanks may be cool, heat transfer will cause temperature increases with corresponding pressure increases. The subsequent burn, then, with higher than nominal tank pressures, will produce higher than nominal chamber pressure and thrust until the propellant ullage pressures decay to the regulator level.

A simulation run will continue until one of two conditions are met. Spacecraft velocity change can be input and total burn time will be determined or burn time can be specified to determine the spacecraft velocity increment.

Malfunction analyses can be made by reflecting in PSOP some physical condition. For example, a hydraulic resistance increase can be used to simulate a blockage or a tank pressure reduction can show the effect of leakage in some component.

II. *Viking* Project, Orbiter System and Project Support

A. Project Description and Status

1. Description

The primary objective of the *Viking* Project is to send two vehicles to the planet Mars to perform scientific experiments directed toward enhancing current knowledge about the physical characteristics of the planet, particularly its capability for supporting life and possible evidence of life. The two vehicles, each consisting of an orbiter system and a lander system, are anticipated for launch during 1975. The orbiter system will be developed by JPL, and the lander system will be developed by the Martin-Marietta Corp. Langley Research Center has overall management responsibility for the *Viking* Project.

The orbiter system will transport and inject the lander system at the appropriate point for a selected landing site and will relay telemetered data from the lander to earth. Scientific instruments on the orbiter will be used to measure atmospheric and surface parameters at various times and locations to determine the dynamic characteristics of the planet. The topography of Mars will be mapped during orbital operations, with special emphasis on mapping the proposed landing site prior to deorbit of the lander system and on supporting the lander after it is on the surface of Mars by determining if changes are apparent in the vicinity of the lander. Both visual and infrared coverage will be possible during the presently planned 140 days of orbital operations.

During entry and after landing, the scientific instruments on the lander will measure Mars' atmospheric composition, temperature, pressure, and density. After landing, the topography of the landing site will be mapped, and measurements will be made of the planet's surface composition, temperature, pressure, humidity, and wind speed. Of particular interest in the surface measurements are the type of organic compounds present, if any, and the amount and form of water. A gas chromatograph/mass spectrometer, for measuring both atmospheric and surface composition, is being developed by JPL. The surface soil analyses will be directed at detecting evidence of growth and/or metabolism.

2. Status

By direction of NASA, the launch, originally scheduled for 1973, was deferred two years to the Mars launch opportunity in 1975. *Viking* mission objectives and implementation remained unchanged from the 1973 plans, although significant differences exist in trajectories, mission duration, and communications distances. Consequently, the major areas of activity presently defined for JPL are:

(1) Emphasis on the 1975 mission design.

(2) Support of Project level documentation.

(3) Orbiter system level design.

(4) Preparation for issuance of subsystem contracts in late 1971.

(5) Involvement with the recently authorized *Mariner* Venus–Mercury 1973 Project to achieve a high degree of hardware commonality at the subsystem and electronic assembly level.

Overall mission definition investigations were initiated in January and February 1970 to assess the full impact of the new launch date.

B. Space Sciences

1. Dynamic Response of a Gas Chromatograph–Mass Spectrometer Combination

a. Introduction. The purpose of this analysis is to establish the required static sensitivity that a mass spectrometer must have for a given mass flow rate into the mass spectrometer, mass scan rate, mass scan range, and signal-to-noise ratio. A flat top peak is assumed and an electrometer time constant is specified. The major noise source is shot noise at the first dynode of the electron multiplier. There is a shot-noise component for both the dark current and the signal current.

The sample mass flow rate into the ion source is limited by the source conductance and a maximum source pressure of 10^{-4} torr. The mass analyzer pressure is held at a much lower pressure by a vacuum pump. The spectrometer sensitivity is specified at the first dynode of the multiplier. To relate the sensitivity to the ion source, the transmission efficiency of the analyzer must be obtained.

This analysis is intended to be general. The generality is maintained by not considering the transmission efficiency of the analyzer and by restricting the mass scan rate to those values at which the shot-noise component of the signal current is much larger than the shot-noise component of the dark current. Some of the desired generality of the analysis is impossible because the time function of the mass scan must be known. For this reason, the required sensitivity is given for a number of mass–time functions. The following cases are considered:

(1) Mass is a linear function of time.

  (a) Constant base width of a mass peak.

  (b) Constant resolving power.

(2) Mass is an exponential function of time.

  (a) Constant resolving power.

(3) Scan voltage is a linear function of time.

  (a) Constant resolving power.

Cases 1a and 1b are common to a quadrupole mass spectrometer, while a magnetic spectrometer can utilize case 1b only if the scan voltage is a hyperbolic function of time. For a quadrupole instrument, cases 1b and 3a are identical; but for a magnetic instrument, they are different. Case 2a is most commonly used with a magnetic mass spectrometer.

The required electron multiplier gain is given as a function of minimum output voltage for the electrometer, electrometer time constant, and the required minimum ion current to the first dynode.

b. System analysis. The throughput Q for a gas chromatograph is related to the mass flow rate by

$$Q = \frac{R_0 T}{M} \frac{dm}{dt}$$

where

R_0 = 67.36 torr-liters/°K g-mole

T = absolute temperature

M = molecular weight

m = mass

t = time

For a closed-ion source, the source pressure is given by

$$P_S = \frac{Q}{F_S}$$

where

F_s = source conductance

The shot-noise current of a multiplier is given by

$$i_N = [2e\Delta f(i_s + i_t)]^{1/2}$$

where

i_s = signal current

i_t = thermionic emission current of the first dynode

Δf = bandwidth of the electrometer

e = electronic charge

The minimum ion current that can be detected is given by

$$I_r = e\Delta f\left(\frac{i_s}{i_N}\right)^2 \left\{1 + \left[1 + \frac{2i_t}{e\Delta f}\left(\frac{i_N}{i_s}\right)^2\right]^{1/2}\right\} \simeq 2e\Delta f\left(\frac{i_s}{i_N}\right)^2$$

if

$$i_t < \frac{e}{2}\Delta f\left(\frac{i_s}{i_N}\right)^2$$

$$\Delta f = \frac{1}{\tau_a}$$

where

τ_a = time constant of the electrometer

The time required to sweep across one mass peak is given by

$$\tau_P = \frac{\tau_S}{M_2 - M_1}$$

where

τ_S = spectrum scan line

M_2 = upper mass limit

M_1 = lower mass limit

$\Delta M = M_2 - M_1$

If the top of the peak is assumed to be 0.1 of the base and if the electrometer should stabilize half way across the top, then

$$\tau_a = 0.05\tau_P = 0.05\frac{\tau_S}{\Delta M}$$

$$\Delta f = 20\frac{\Delta M}{\tau_S}$$

$$I_r = 40e\frac{\Delta M}{\tau_S}\left(\frac{i_s}{i_N}\right)^2 \quad \text{(Fig. 1)}$$

$$i_t < 10e\frac{\Delta M}{\tau_S}\left(\frac{i_s}{i_N}\right)^2 \quad \text{(Fig. 2)}$$

The required sensitivity is given by

$$S_e = \frac{I_r}{P_s} = 40e\frac{\Delta M}{\tau_S}\frac{\left(\frac{i_N}{i_s}\right)^2 F_s M}{R_0 T\frac{dm}{dt}}$$

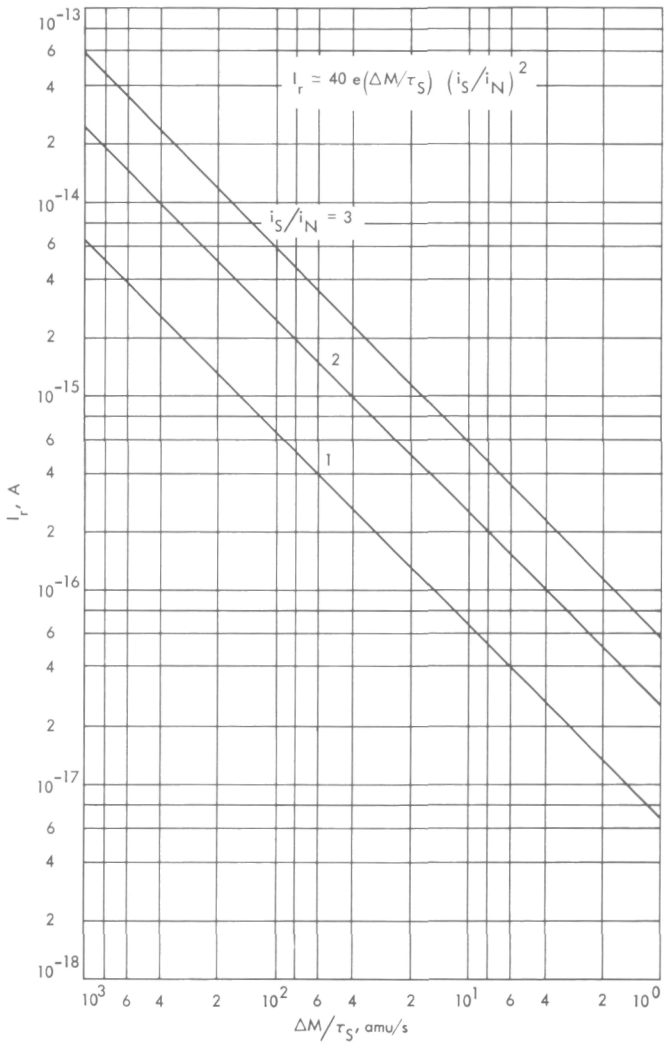

Fig. 1. Required minimum current

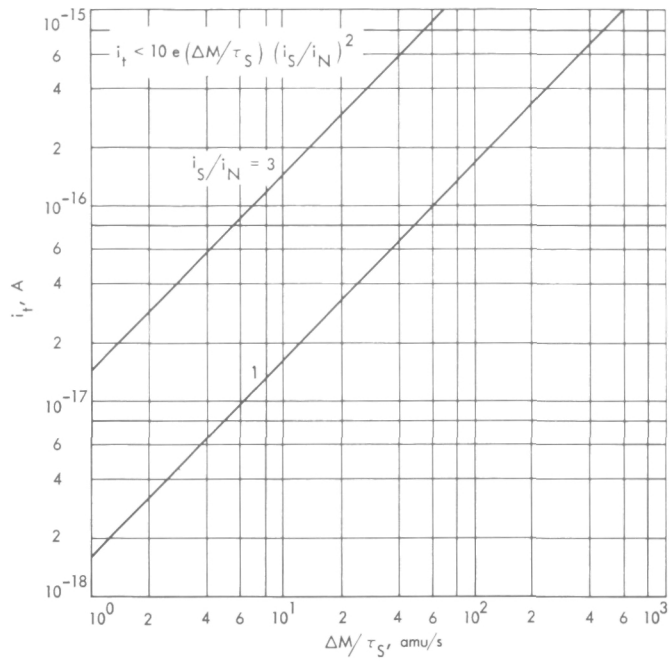

Fig. 2. Maximum noise current

where

$$F_S = \left(\frac{1}{4}\right) A_c v_a K$$

$$K = \frac{1}{1 + \left(\frac{3}{8}\right)\frac{L}{t_0}}$$

L = length of the source exit slit

t_0 = thickness of the source exit slit

A_c = cross sectional area of the source exit slit

$$v_a = \left(\frac{8R_0T}{\pi M}\right)^{1/2}$$

Thus,

$$S_e \simeq \frac{20\left(\frac{2}{\pi}\right)^{1/2} Ke\,\frac{\Delta M}{\tau_S}\left(\frac{M}{R_0T}\right)^{1/2}\left(\frac{i_S}{i_N}\right)^2}{\frac{dm}{dt}} \qquad \text{(Fig. 3)}$$

The electrometer time constant must be related by

$$\tau_a = R_f C_f$$

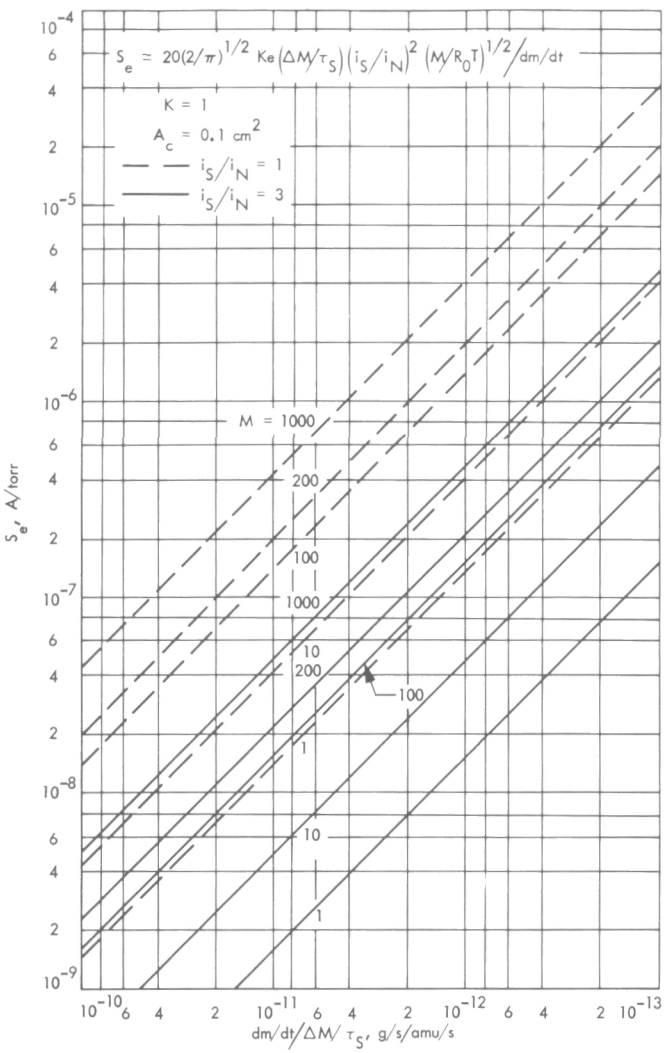

Fig. 3. Required sensitivity

where

R_f = feedback resistor

C_f = shunt capacitance of the feedback resistor

The minimum output voltage from the electrometer is

$$V_{min} = R_f I_r G_m$$

where

G_m = gain of the electron multiplier

Thus,

$$G_m = \frac{V_{min}C_f}{\tau_a I_r} = \frac{V_{min}C_f}{\tau_a\left[\frac{e}{\tau_a}\left(\frac{i_S}{i_N}\right)^2\right]} = \frac{V_{min}C_f}{e\left(\frac{i_S}{i_N}\right)^2} \qquad \text{(Fig. 4)}$$

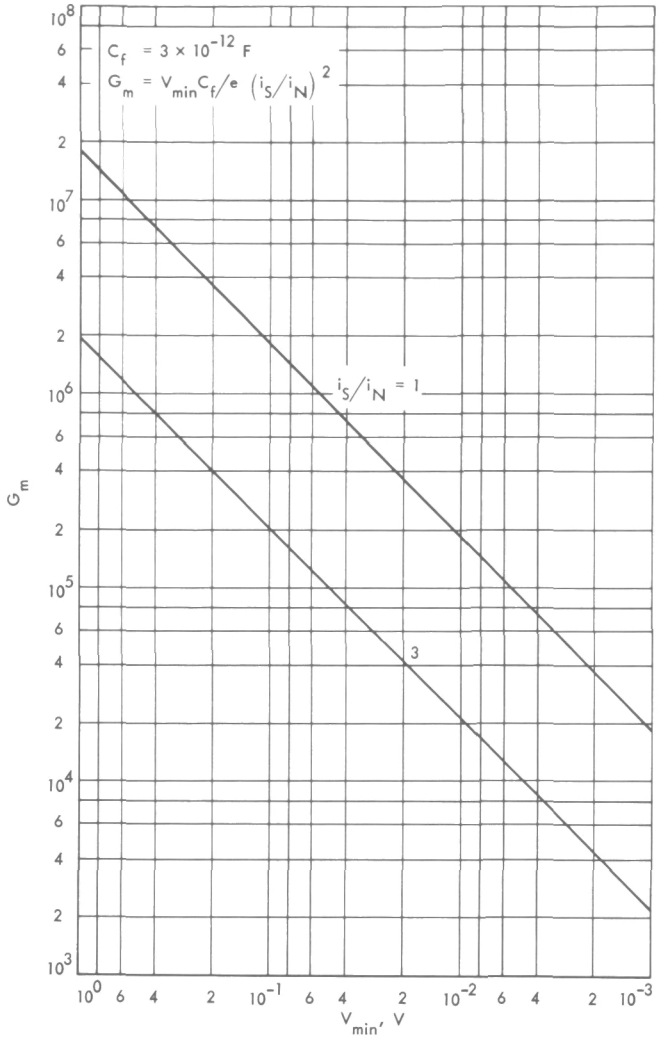

Fig. 4. Required multiplier gain

For a double-focused mass spectrometer, $\Delta m \neq 1$ amu; therefore, the sensitivity is not the same as for the quadruple mass spectrometer. Three types of scan functions will be considered:

(1) Hyperbolic—voltage varies inversely with time.

(2) Exponential.

(3) Linear—voltage decreases linearly with time.

The required sensitivity is given by

$$S_e \simeq \frac{10\left(\frac{2}{\pi}\right)^{1/2} \frac{K}{\Delta t_b}\left(\frac{M}{R_0 T}\right)^{1/2}\left(\frac{i_S}{i_N}\right)^2}{\frac{dm}{dt}}$$

Hyperbolic

$$M = \frac{\Delta M}{\tau_S} t$$

where

ΔM = difference between the high mass and the low mass

τ_S = time required to scan

The time across the base is

$$\Delta t_b = \frac{M}{R} \frac{\tau_S}{\Delta M}$$

where

$$R = \frac{M}{\Delta m}$$

Δm = base width of a mass peak

The time between adjacent peaks is

$$\Delta t_P = \frac{\tau_S}{\Delta M}$$

Thus,

$$S_e = \frac{20\left(\frac{2}{\pi}\right)^{1/2} \frac{KR}{(MR_0T)^{1/2}} \frac{\Delta M}{\tau_S}\left(\frac{i_S}{i_N}\right)^2}{\frac{dm}{dt}} \quad \text{(Fig. 5)}$$

Exponential

$$M = M_1 \exp\left(\frac{t}{\tau_S} \ln M_R\right)$$

where

$$M_R = \frac{M_2}{M_1} = \frac{M_1 + \Delta M}{M_1} = 1 + \frac{\Delta M}{M_1}$$

and

$$\Delta t_b = \frac{\tau_S}{R \ln M_R}$$

$$\Delta t_P = \frac{\tau_S}{M \ln M_R}$$

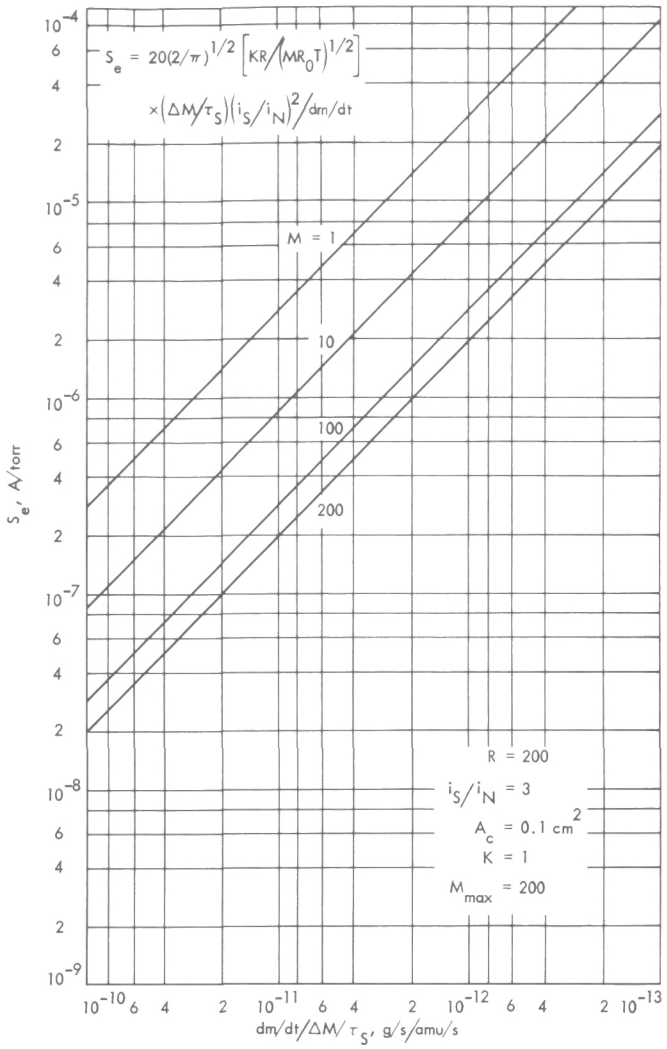

Fig. 5. Hyperbolic scan

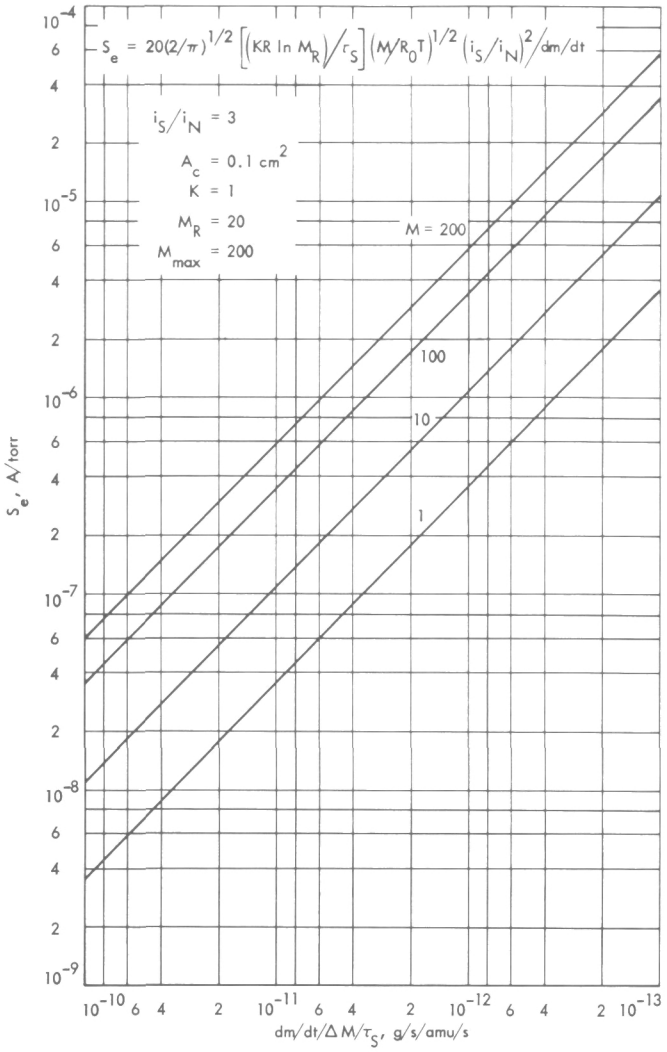

Fig. 6. Exponential scan

Thus,

$$S_e = \frac{20\left(\frac{2}{\pi}\right)^{1/2}\frac{KR\ln M_R}{\tau_S}\left(\frac{M}{R_0T}\right)^{1/2}\left(\frac{i_S}{i_N}\right)^2}{\frac{dm}{dt}}$$

(Fig. 6)

Linear voltage scan

$$M = \frac{M_1}{\left[1 - \frac{t}{\tau_S}\left(1 - \frac{1}{M_R}\right)\right]}$$

and

$$\Delta t_b = \frac{M_1}{RM}\,\frac{\tau_S}{\left(1 - \frac{1}{M_R}\right)}$$

$$\Delta t_P = \frac{\tau_S}{(M_1 + 1)\left(1 - \frac{1}{M_R}\right)}$$

Thus,

$$S_e = \frac{20\left(\frac{2}{\pi}\right)^{1/2} K\frac{R}{M_1}\,\frac{\left(1 - \frac{1}{M_R}\right)}{\tau_S}\,\frac{M^{3/2}}{(R_0T)^{1/2}}\left(\frac{i_S}{i_N}\right)^2}{\frac{dm}{dt}}$$

(Fig. 7)

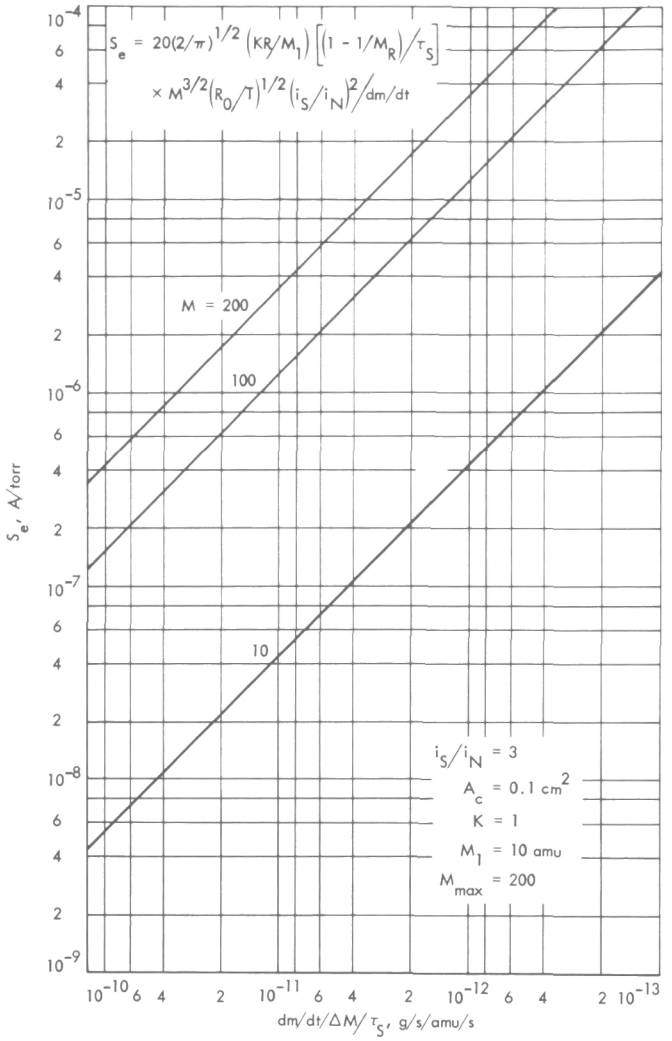

Fig. 7. Linear voltage scan

c. Conclusions. A sensitivity of 2×10^{-6} A/torr at the input to the multiplier would allow a sample flow of 10^{-11} g/s, with a scan from mass 12 to 200 in 10 s, with a signal-to-noise ratio of 3.

For the double-focused mass spectrometer, the hyperbolic scan seems to be the best since it requires the highest sensitivity at the lighter mass, where the most efficient transmission is obtained.

C. Guidance and Control

1. Effects of Propellant Slosh Dynamics on *Viking* Orbiter Powered Flight Control

a. Introduction. Propellant sloshing is a potential source of spacecraft disturbances that may adversely affect the stability of the flight control system, particularly during powered flight phases of the mission.

Sloshing refers to the free surface oscillations of a fluid in a partially filled tank. These oscillations result from lateral and longitudinal displacements or angular motions of the spacecraft.

This article summarizes the results of a preliminary analysis that was made to model the effects of propellant slosh dynamics on the *Viking* spacecraft during powered flight control.

b. Discussion. Current *Viking* spacecraft designs envisage a liquid propulsion system with propellant loads on the order of 50% of the total planetary vehicle mass. Sloshing, therefore, is expected to be a potential source of disturbances.

The effects of propellant slosh dynamics were analyzed through the use of an equivalent mechanical model, consisting of masses and springs, which was generated from a system of linearized dynamic equations of propellant motion. The analysis leading to the development of this equivalent mechanical model assumed that (1) viscous and surface tensions forces may be neglected, (2) the propellant responds only to purely lateral input excitations, (3) propellant motion can be described as small-amplitude forced oscillations, and (4) the regime of propellant motion is dominated by gravity force (powered flight).

The formulation of this equivalent mechanical model for propellant slosh is based on the original work done by JPL for the *Voyager* Project. The propulsion system that was envisaged for the *Voyager* spacecraft utilized LEMDS[1] propellant tanks. The *Viking* spacecraft propellant tanks have the same basic geometry as the LEMDS tanks so that the analysis originally done for *Voyager* was easily adapted to *Viking*. The details of the original propellant slosh analysis and the generation of the equivalent mechanical model are described in Ref. 1.

Figure 8 shows, diagrammatically, the equivalent mass spring model used for the *Viking* orbiter propellant slosh analysis. As derived in Ref. 1, this model was generated from the linearized dynamic equations of propellant motion, subject to the assumptions stated above and the constraints imposed by the boundary conditions which

[1]LEMDS = lunar excursion model descent stage.

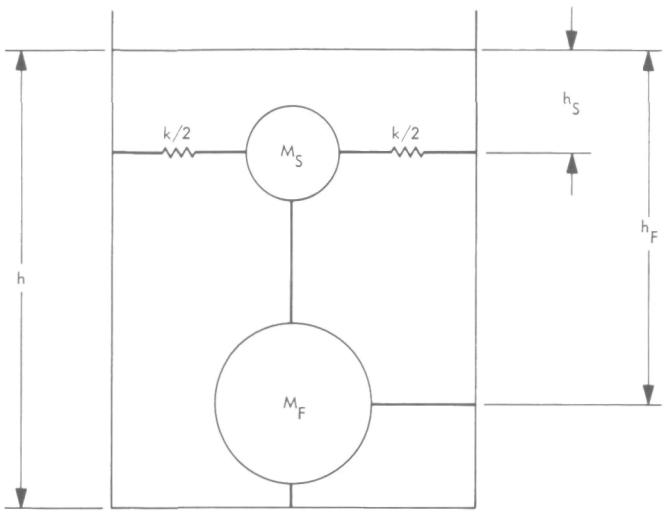

Fig. 8. Cylindrical tank and equivalent mechanical model

were determined from the specific geometry of the *Viking* orbiter propellant tanks.

The model shown in Fig. 8 depicts the fluid dynamic system as an equivalent undamped (no baffles) spring mass system. The propellant in the tank is considered to be made up of two parts: (1) a fixed propellant mass M_F whose motion is constrained with respect to the tank, (2) and a slosh propellant mass M_S whose motion relative to the tank is governed by an associated spring constant k.

These parameters are dependent on the total mass of propellant remaining in the tank and are, therefore, time-dependent during powered flight phases of the mission. The propellant (fuel and oxidizer) for the *Viking* spacecraft is contained in two identical cylinderical tanks along the spacecraft pitch axis and equidistant from the spacecraft roll axis. The propellant slosh equations of motion, based on the model depicted in Fig. 8, were incorporated into an existing six-degree-of-freedom autopilot and spacecraft dynamics computer simulation program.

c. Computer simulation. Some typical results of the computer simulation are shown in Figs. 9 through 12. Figures 9 and 10 show the displacements of the oxidizer and fuel slosh masses in the X (pitch) and Y (yaw) directions within their respective tanks during a simulated engine burn. In the simulation, the engine is ignited at $t = 2.0$ s and burns until $t = 30.0$ s. This simulated burn is representative of a midcourse or the beginning of an orbit insertion burn. The undamped natural frequency of the slosh masses is 0.20 Hz so that they oscillate within the tanks with a period of 5.0 s. The largest peak-

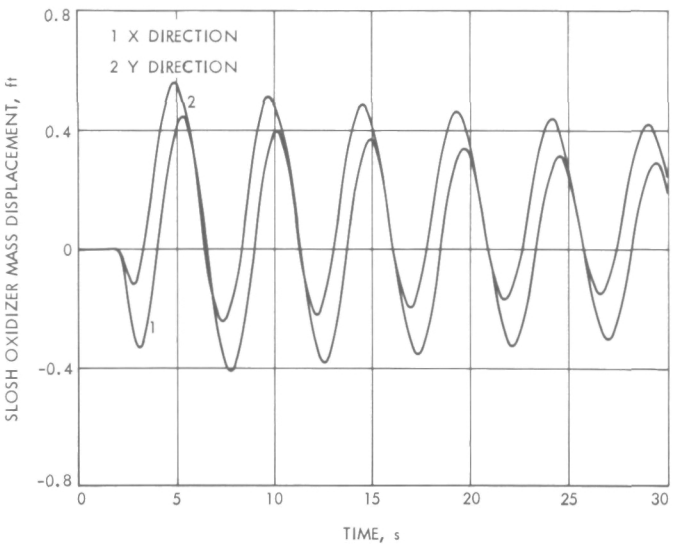

Fig. 9. Slosh oxidizer mass displacement vs time

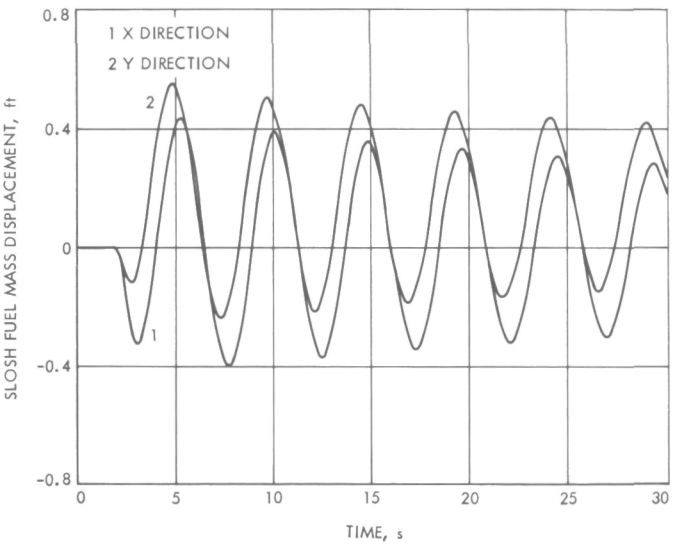

Fig. 10. Slosh fuel mass displacement vs time

to-peak amplitude is 0.08 ft in the X direction. The only damping in the system is contributed by the autopilot control system. With regard to autopilot performance, the effect of these oscillating slosh masses is negligible. This can be seen in Fig. 11, which shows the engine yaw gimbal position during the burn. The yaw gimbal deflection corresponds to an initial engine to center-of-mass misalignment in the X direction. Since the slosh natural frequency is within the passband of the autopilot, the autopilot response will exhibit a low amplitude oscillation at this frequency. The effect on pointing error is shown in Fig. 12. The initial transient is due solely to the initial misalignment with the center-of-mass and

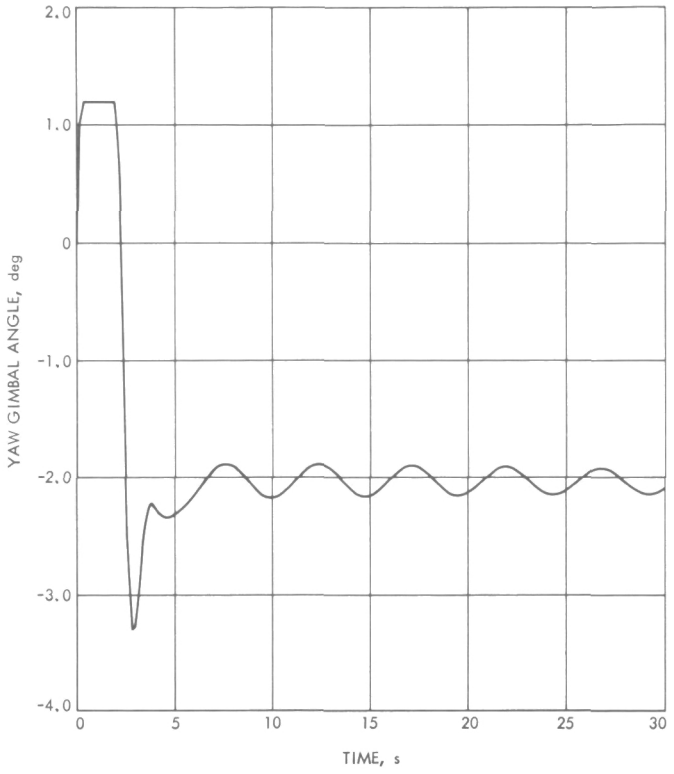

Fig. 11. Yaw gimbal angle vs time

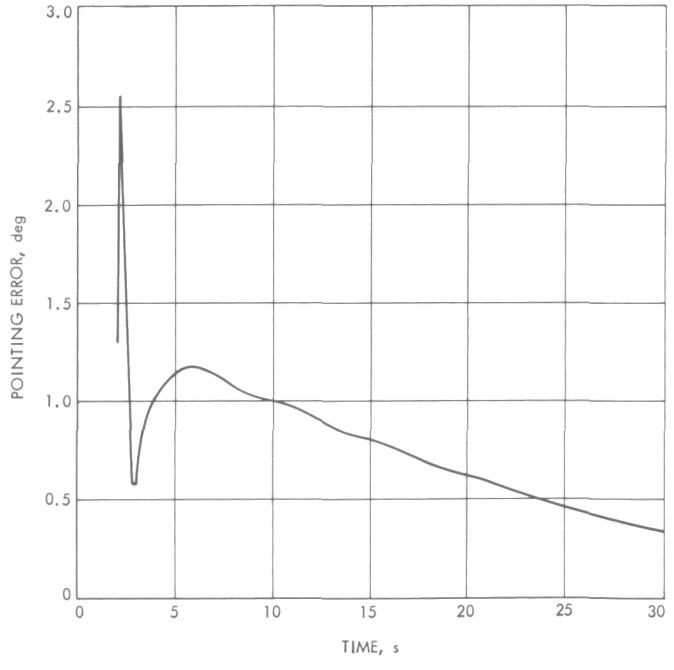

Fig. 12. Pointing error vs time

autopilot transient response characteristics. Propellant slosh, as modelled here, has no effect on steady-state pointing accuracy.

d. Conclusion. The simulated autopilot and vehicle response characteristics during powered flight are based on a propellant fluid dynamic system, which can be described by a simple linear mass-spring equivalent mechanical model. Use of this equivalent mechanical model is the first attempt to analyze the effects of propellant slosh dynamics as a potential source of disturbance to the *Viking* orbiter spacecraft during powered flight phases.

The results of the analysis, for the system modeled as described in this article, indicates that autopilot stability and response are virtually unaffected by propellant motion. However, considerably more work must be done to better understand and model the dynamic behavior of propellant motion. For example, the current *Viking* orbiter propellant tank design does not incorporate bladders. This means that the propellant dynamic system is essentially unconstrained and contains no damping. Although the present model considers the case of no damping, it does not adequately describe the case of large amplitude propellant motion and does not describe the case of longitudinal and pitching motion. Of even greater concern is the case where a large portion of the propellant has migrated away from the center of the tank due to the zero-*g* environment prior to the initiation of a powered flight phase. This situation can give rise to prohibitively large shifts in the vehicle center of mass and result in severe start transients at engine ignition.

Future effort in this area will be directed at developing a more complete dynamic model which can be used in conjunction with existing computer simulation programs to analyze propellant motion and the resulting disturbance effects.

Reference

1. Lance, T. A., "Analysis of Propellant Slosh Dynamics and Generation of an Equivalent Mechanical Model for Use in Preliminary *Voyager* Autopilot Design Studies," Technical Memorandum 33-306. Jet Propulsion Laboratory, Pasadena, Calif., Dec. 1, 1966.

D. Engineering Mechanics

1. Introduction

The configuration of the 1973 *Viking* orbiter was described in SPS 37-59, Vol. I, pp. 38–41, and SPS 37-60, Vol. I, pp. 44–45. In the following discussion, the configuration description is brought up to date, reflecting

changes which have occurred as the orbiter design has developed. In addition, the considerations which led to the current arrangement of the electronics within the orbiter are discussed in more detail.

A key element of the thermal design, a device named a solar energy controller (SEC), is also discussed. The device is described and the results of the initial feasibility studies and tests are summarized.

2. Configuration Description

Of the twenty subsystems currently identified as part of the *Viking* orbiter, six have caused changes in the configuration (Fig. 13). They were the power, attitude control, propulsion, structure, S-band antenna, and temperature control subsystems. Other changes have occurred, but either they have not affected the mechanical configuration of the orbiter or they are not considered sufficiently defined to be included in this article.

a. Power subsystem. The total solar panel area has been increased from 115 to 158 ft^2, resulting in the addition of two additional solar panels (Fig. 13). This change from 4 to 6 solar panels also affected the location of the S-band antennas, the attitude control sensors, and caused a complete revision of the location of the electronic assemblies within the orbiter. Several factors contributed to the increase in solar panel area: (1) an increase in orbiter temperature control subsystem power requirements, (2) a decrease in panel performance based on *Mariner VI* and *VII* flight experience, (3) the extension of mission lifetime, (4) a further requirement that the lander may be attached to the orbiter up to 50 days beyond orbit insertion, and (5) the requirement that science playback will be possible during battery charging periods.

b. Attitude control subsystem. The relocation of the attitude control bottles and celestial sensors was made both possible and necessary by the change from the four-tank to the two-tank propulsion module described in SPS 37-60, Vol. I, pp. 45–49. The current two-tank design makes four previously unusable small bays in the orbiter ideal locations for the attitude control nitrogen bottles, the Canopus tracker, and the stray light sensors.

Each of the two parts of the gas system can now be made identical and installed as a completely welded and checked out assembly to the spacecraft. In addition, the gas bottles and regulators, as is the case with the Canopus tracker, are within the controlled temperature environment of the orbiter bus.

c. Propulsion subsystem. The expansion ratio of the engine nozzle was changed from 40:1 to 60:1 to increase the specific impulse of the engine by 4 s, and a gas plumbing plate was added to the propulsion module structure to provide a support for pressurant control components. A "nerfing bar" structure has been added to the end of the propellant tanks nearest the engine to support the thermal shield and maintain noncontact between the shield and the tanks.

d. Structure subsystem. A slightly different configuration of the launch-vehicle-to-spacecraft adapter occurred as part of the change from the four-tank to the two-tank propulsion module. An analysis of this truss indicates that the upper ring, which tied the four attachpoints to the spacecraft together, was not required. This was probably also true with the earlier design, but the definition of the bus and adapter was not known well enough to recognize this advantage. With the removal of this structural ring at the top of the launch-vehicle-to-spacecraft adapter, it was possible to relocate the low-gain antenna so that an in-flight deployment was not required.

The scan platform was relocated to an off-center position near the $+y$ axis. This was easier to support with the new two-tank propulsion module design and provided a greater unobstructed view for the science instruments while the lander capsule was still aboard the orbiter.

e. S-band antenna subsystem. The 58-in.-diameter high-gain antenna was moved from a position 270 deg from the Canopus tracker to a position 180 deg from it. This was part of the change from four to six solar panels but is not a significant change to the subsystem. A known change to a combined S-band/X-band antenna has not been included in the configuration, but a drawing correction of the focus-to-diameter ratio was made (0.260 to 0.3795) to show the proper location of the S-band feed assembly. The maneuver antenna was defined and was moved from a position on the $-x$ solar panel to the $+x$ solar panel outrigger for better earth coverage during the orbit insertion maneuver.

f. Temperature control subsystem. Figure 13 shows the location of some of the thermal blankets and for the first time the locations of the four solar energy controller devices. These devices are, in effect, thermal greenhouses which trap solar radiant energy for maintaining the temperature of the propulsion module. Preliminary experi-

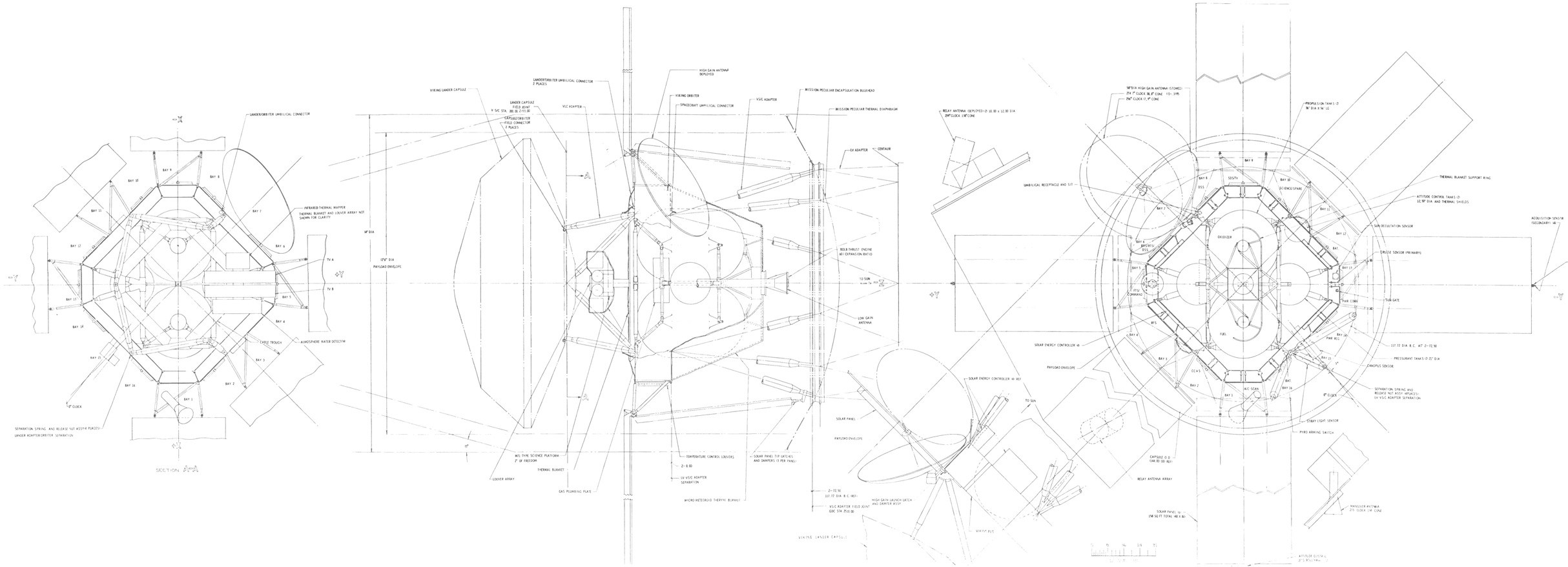

Fig. 13. *Viking* orbiter configuration

Page intentionally left blank

ments, discussed later in this article, indicate that this use of the solar energy for heating is under certain conditions an order-of-magnitude more efficient than electrical heaters which are powered by solar panels.

3. Electronic Equipment Layout

The *Viking* orbiter spacecraft octagonal structure contains subsystem electronic equipment within semi-standardized electronic assemblies (EAs). Flight hardware from a minimum of three subsystems (flight cabling, structure, and subassemblies from an electrical subsystem) are contained within an EA. Electronic subassemblies from as many as six subsystems are contained within a single EA in some instances. The placement of electronics within EAs and the location of EAs within the spacecraft octagonal structure involve a study of temperature control, flight cabling, cabling weight and center of gravity, and electronic subsystem considerations. Figure 14 shows the *Viking* electronic equipment layout as of January 1970. While the location of the equipment is an iterative process during the early phases of the orbiter development, the following discussion is intended to outline some of the major considerations that form a basis for the present configuration.

a. Temperature control. The spacecraft octagonal section (bus) is divided thermally into two approximately equal areas by the propulsion module (Fig. 14). Temperature control design considerations indicate that the dissipated power within the bus should be balanced across a plane cutting through the propulsion tanks because of the thermal isolation effect of the tanks. Radiant heat exchange within these two general areas is expected to be adequate, but from one area to the opposite one, the radiation will be blocked by the propulsion tanks.

In addition, it was desired to exclude high-power dissipating EAs from both bays 1 and 9 (Fig. 13), because the close proximity to the propulsion module might result in an excessively hot spot on a tank. Excluding bays 1 and 9, the average power dissipation on the $+y$ side of the propulsion module is 187.7 W and on the $-y$ side is 121.2 W. This difference appears to be more than desired from a purely thermal point of view; however, the unbalance is largely due to the high-power dissipation of the radio. Because of its high power, it is necessary to radiate most of the heat of the radio assembly directly to space, and this outboard-radiated heat is lost for purposes of maintaining the overall spacecraft temperatures. The result is that an almost equal balance in the power layout dissipated within the two areas of the bus exists with the layout shown.

Additional desirable spacecraft thermal characteristics are obtained by alternately locating EAs of high- and low-power dissipation in bays of the octagonal structure to promote heat transfer between adjacent units by conduction. The location of the EA within the octagon also considers the external appendages of the spacecraft, such as the solar panels and the high-gain antenna, which block off line-of-sight areas of space used for the external radiation heat sink.

b. Flight cabling. The same technical considerations are studied for subsystem cabling that are used for system cabling. General cabling considerations include minimization of weight, optimization of electrical performance and reliability, electromagnetic interference protection of susceptible circuits, isolation of noise-generating circuits, and control of voltage drops and/or power losses. System cabling constraints take into account these considerations in the cabling design of the entire spacecraft and the electrical interconnection of the various flight equipment subsystems. The design of subsystem cabling within each EA is a major factor in the location of electronic subassemblies.

The radio assembly was the most difficult EA to locate in the bus because of conflicting cabling and thermal considerations. Cabling constraints indicated that bay 6 was the most desirable location for the radio because of the close proximity to the high- and low-gain antennas, and to the flight telemetry subsystem. Based only on thermal considerations alone, bay 14 would have been the best location because it is not too close to a propulsion tank and provides a maximum view of space for radiative heat rejection. Bay 4 was finally selected for the radio assembly after considering all the trade-offs. In this location, the desirable close proximity to the flight telemetry subsystem is maintained; the outboard view of the radio assembly is partially blocked by the adjacent solar panels, but thermally the location is acceptable for the 20-W RF output of the radio assembly, and bay 4 is also close enough to the two antennas so that the RF power loss in the co-axial transmission lines is not excessive.

Cabling considerations had a strong effect on the relative locations of the two battery assemblies, the power regulator assembly, and the power conversion subassemblies. The power regulator assembly and the power conversion subassemblies should be adjacent because of the

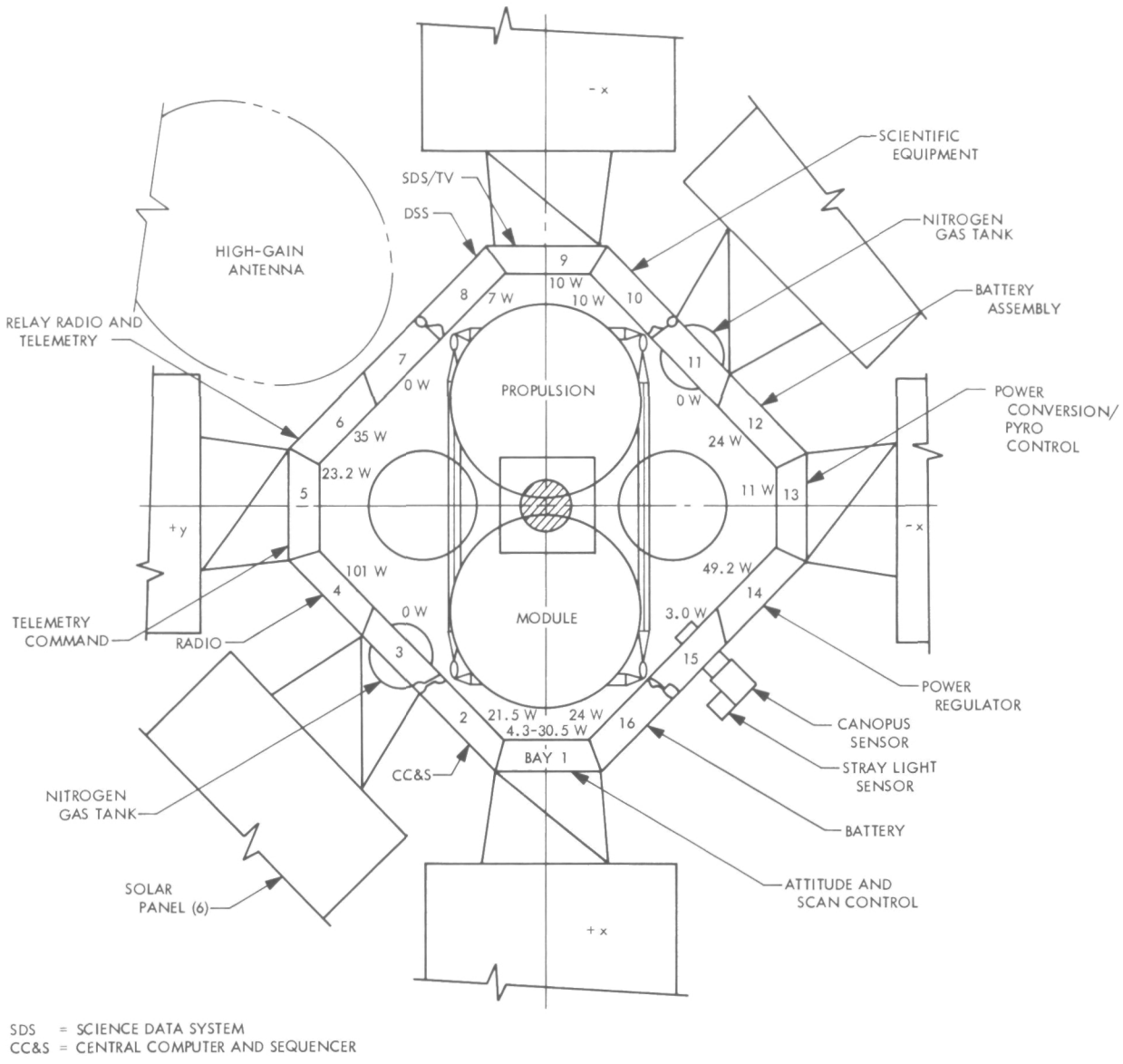

Fig. 14. *Viking* orbiter electronic equipment layout

extensive number of conductors required to interconnect the two assemblies. Another cabling consideration indicated that the battery assemblies should be close to the power regulator EA, and that the distances from each of the two batteries to the power regulator EA should be approximately equal to balance the voltage drops during time periods when the batteries were being used. The power equipment was, therefore, laid out as a group, as shown in Fig. 13 (Bays 12–16), and all of the above-mentioned requirements were satisfied without the compromise of any other major consideration.

There was also an attempt to locate the radio, command, telemetry, and data storage equipment in such a way as to minimize the number and length of the interconnecting cables. This was of particular concern where signal cables were involved. The data storage EA (in bay 8) was located adjacent to the TV subassemblies (located in bay 9) because of the critical nature of the signals transmitted from the TV to the data storage subsystem.

c. Cabling weight and center of gravity. The weights of the EA were considered as the EA locations were established; within bays in the octagonal structure, the average distance between the center of gravity of the EA and the spacecraft z-axis is approximately 44 in. and the differences in weight and relative location of the EA

have a significant effect on the overall spacecraft center of gravity. Although incomplete weight information is available at this time, it is anticipated that the battery assemblies and the radio assembly will be heavier than EAs with more standard electronics, and Fig. 14 shows that these three heavy assemblies tend to balance out the high- and low-gain antennas.

d. Electronic subsystem considerations. Groups of electronic subassemblies functioning as complete subsystems are located in a single EA whenever possible; the advantages of this approach are somewhat obvious: (1) subsystem testing is simplified, (2) electrical performance is improved, (3) cabling design constraints are simplified, (4) handling and shipping are easier, and (5) project costs are reduced. Only the power subsystem flight equipment is not contained within a single EA; the power subsystem requires the volume of 3½ EA for flight electronic equipment.

Two of the "small" bays (3 and 11) were also utilized to a temperature control and packaging advantage by locating the attitude control nitrogen gas bottles in these areas. These two bays are symmetrical with respect to the primary spacecraft z-axis and the solar-panel-mounted gas jets, thus allowing the entire gas system to be designed, fabricated, and installed as two identical redundant welded systems.

The attitude and scan control EAs were located in bay 1 primarily to position the gyro subassembly on one of the primary axes of the spacecraft. This simplified the control logic and maintained a no-change design from the *Mariner* Mars 1971. The Canopus sensor and stray light sensor were located in bay 15, where there is no solar panel, to minimize the possibility of stray light being reflected into the sensors. Although this location is not adjacent to the attitude control bay, it is in fairly close proximity. There was a temperature control advantage in locating the sensors in the small bay 15 rather than on the upper ring shown in previous configurations in that the thermal blanket design was simplified. When power, weight, and even organizational conditions become better defined, adjustments in the packaging layout can be anticipated to provide optimized design flexibility to the spacecraft development process.

4. Solar Energy Controllers

Four solar energy controllers (SECs) mounted at the bus/propulsion module blanket interface will regulate solar energy into the propulsion module for temperature control purposes. By being independently controlled from the ground through the flight command subsystem, the SEC will not only maintain the propulsion module at a desired average temperature, but will also minimize the thermal gradients expected in the propulsion module. Briefly, the SEC is a shuttered greenhouse window. The greenhouse window is transparent to the solar energy allowed through the shutters and opaque to the infrared energy emitted from within the orbiter. Application of the greenhouse technique has varied from indoor winter gardening to a possible explanation of the high temperature of the surface and lower atmosphere of Venus. In the latter example, a portion of the atmosphere acts as the greenhouse window and prevents further cooling of the planet. A feasibility model of the SEC, referred to as the *Viking* 1973 greenhouse, has been tested in a small cold-wall vacuum chamber. The analytical and test results relative to this effort are summarized in the following discussion.

a. Feasibility model. For the flight model, the plane of the window is approximately in line with the sun. Articulated louvers, normal to the sun in the closed position, regulate solar energy onto a highly reflective surface. The energy reflected from the surface passes through the window and is reflectively spread onto the propulsion tanks, structure, etc. The feasibility model was representative of this type of a system.

The model is shown mounted in the vacuum chamber in Fig. 15. Briefly, the model consists of a cylindrical aluminum can insulated on the sides and top. A constant amount of energy was purposely radiated from the thermally gray bottom exterior. The inside of the can was thermally black except for a highly polished cone

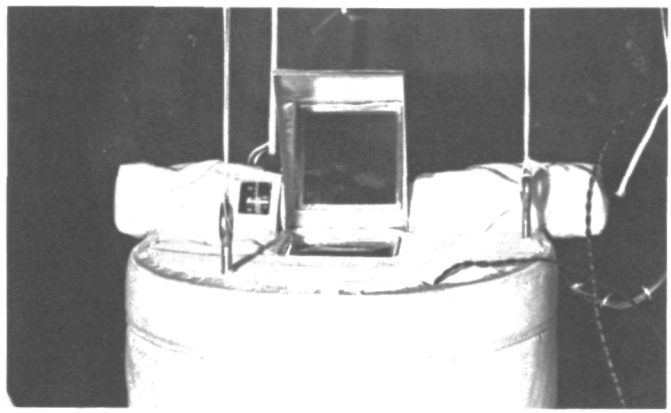

Fig. 15. Greenhouse feasibility model

mounted directly beneath the window to reflect the incoming energy onto the highly absorptive sides of the can. Heaters mounted on the side walls of the can maintained a constant greenhouse temperature. As the remotely controlled door covering the window was opened and the energy reflected into the can, the heater power required was manually reduced until a steady-state condition was maintained. The reduction in heater power required relative to the closed position represents the energy capture by the window.

b. Window materials. Several window materials are under study as a part of the SEC total design. For the feasibility model tests, two materials, gold-coated Kapton and Teflon films, were evaluated. Glass was analytically treated for comparison with the tested films and is a candidate window material. Pertinent greenhouse properties of these window materials are compared in Table 1 to those of a perfect window.

Table 1. Comparison of material properties

Property	Glass	Gold-coated Kapton	Gold-coated Teflon	Perfect window
Solar radiation				
Transmissivity	0.92	0.36	0.56	1.00
Absorptivity	0.03	0.39	0.22	0
Reflectivity	0.05	0.25	0.22	0
Infrared radiation				
Sun side				
Transmissivity	0.10	0.01	0.01	0
Emissivity	0.85	0.12	0.19	0
Reflectivity	0.05	0.87	0.80	1.00
Module side				
Emissivity	0.85	0.78	0.74	0

c. Results. Measured and calculated performances of the feasibility model are presented in Fig. 16. A lumped parameter computer model was used to obtain the calculated results. The solar source intensity at the model was approximately equivalent to that at earth. Since the test was to demonstrate feasibility, verification of the actual source intensity was not made and is obviously a potential error in the analytical comparison.

Calculations indicated that the undesired infrared energy from the cooled chamber door and the port for the simulated solar source was an insignificant input

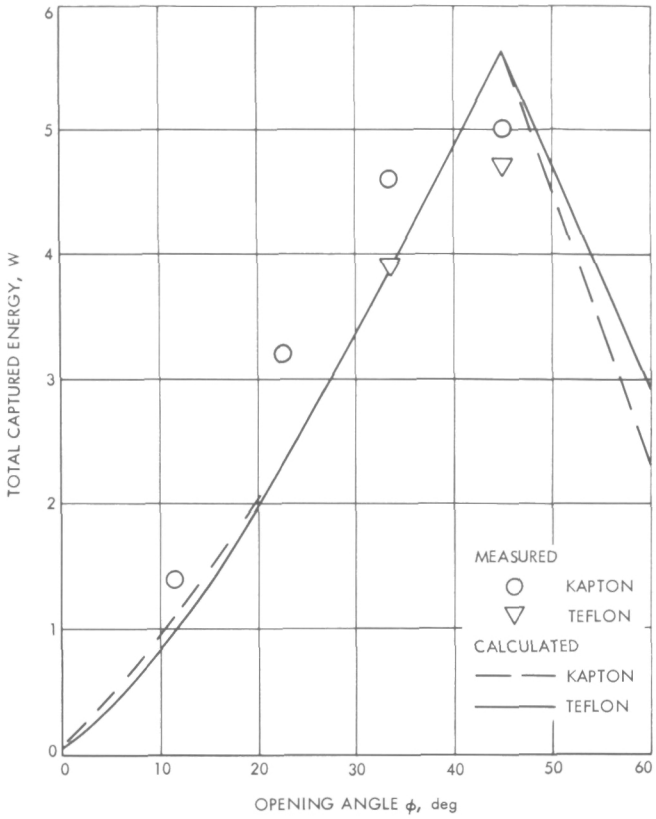

Fig. 16. Greenhouse feasibility model performance

Table 2. Feasibility model calculated capture energy summary

Opening angle, deg	At test intensity			At Mars aphelion		
	Solar energy, W	Infrared energy, W	Total energy, W	Solar energy, W	Infrared energy, W	Total energy, W
Teflon						
0	0	0.03	0.03	0	−0.008	−0.008
15	1.16	0.19	1.35	0.43	−0.214	0.216
30	2.67	0.71	3.38	0.99	−0.008	0.982
45	4.35	1.24	5.59	1.61	0.207	1.817
60	2.38	0.51	2.89	0.88	−0.052	0.828
Kapton						
0	0	0.02	0.02	0	−0.006	−0.006
15	0.76	0.71	1.47	0.281	0.037	0.318
30	1.72	1.66	3.38	0.637	0.402	1.039
45	2.83	2.76	5.59	1.047	0.845	1.892
60	1.26	1.09	2.34	0.464	0.214	0.678
Glass						
45	7.24	−0.66	6.58	2.67	−0.93	1.74

relative to the total energy captured. Analysis also showed that while the total energy captured is approximately the same for two window materials tested (Teflon and Kapton film), the energy transferred in the visual and infrared regions was significantly different, as illustrated by Table 2 for the solar intensities of the test and Mars aphelion.

It is noted that only a small reduction in the infrared loss at Mars would make the performance of the glass better than either of the films. For example, at the 45-deg opening angle at Mars aphelion, the uncoated glass captures 1.74 W (a little less than either film) while losing 0.93 W by IR radiation. If this IR loss is reduced either by the addition of a coating to the glass or reduction in the window view factor to space, the glass would capture more energy than either film. For the currently proposed flight configuration, this latter option is being considered. As a result, an uncoated glass window is expected to perform better than the film materials. However, this increase in performance must still be weighed against the undesirable breakage and weight characteristics of glass.

Other window materials and SEC configurations are being considered, and a means of comparing the performance of each design is necessary. Therefore, an efficiency of capture η_{capt} has been defined as the ratio of the actual energy captured to that which would be captured if a perfect greenhouse window of the same size

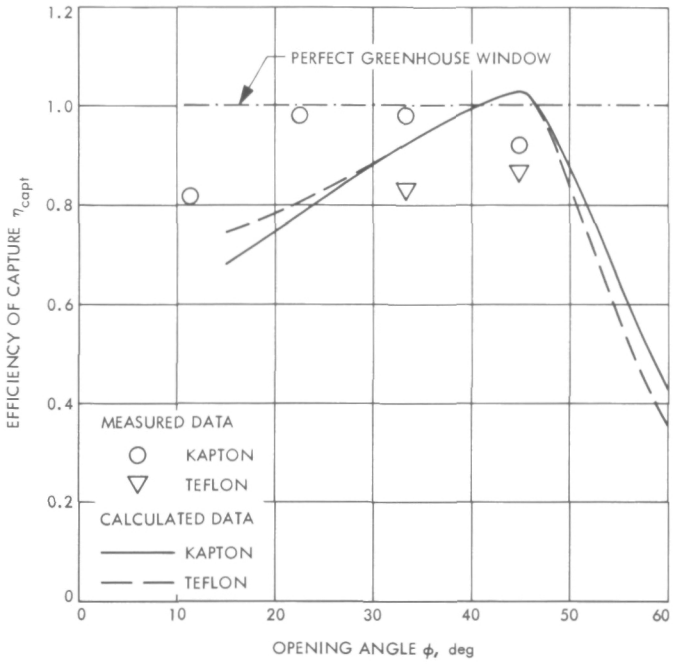

Fig. 17. η_{capt} for greenhouse feasibility model

were exposed directly to the same solar intensity at a sun angle equivalent to the door or shutter opening angle. η_{capt} for the feasibility model tested is presented in Fig. 17. As can be seen in this figure, an η_{capt} greater than 1 is possible by this definition since either a concentrating reflective door or a high infrared emittance (as calculated for the feasibility model) from an oversized door is possible.

Page intentionally left blank

Subject Index

Subject	Pages
Computer Programs	
Mariner Mars 1971 propulsion subsystem operation and performance computer program (PSOP)	22–26
Control and Guidance	
effects of propellant slosh dynamics on *Viking* orbiter system powered-flight control	33–35
***Mariner* Mars 1971 Project**	
project description and status	1–3
television subsystem	3–7
propulsion support structure	7–11
flight cabling	11–13
thermal resistance at spacecraft chassis–subchassis interface	11–12
static test of developmental test model	12–16
modal survey for mathematical model of spacecraft	16–17
spacecraft overturning moment for longitudinal low-frequency environmental vibration test	17–18
metallurgical study of burst-tested propellant vessel	18–19
electronic parts control	19–22
spacecraft propulsion subsystem	22–26
Materials, Metallic	
metals used in *Mariner* Mars 1971 propulsion support structure	7–11
metallurgical study of *Mariner* Mars 1971 burst-tested propellant vessel	18–19
Mechanics	
modal survey for mathematical model of *Mariner* Mars 1971 spacecraft	16–17
Mariner Mars 1971 spacecraft overturning moment for longitudinal low-frequency environmental vibration test	17–18
effects of propellant slosh dynamics on *Viking* orbiter system powered-flight control	33–35
Packaging and Cabling	
Mariner Mars 1971 flight cabling	11–13
Viking orbiter system cabling and electronic equipment layout	39–41
Particle Physics and Nuclear Reactions	
dynamic response of gas chromatograph/ mass spectrometer	28–33
Photography	
Mariner Mars 1971 television subsystem	3–7
Propulsion, Liquid	
metallurgical study of *Mariner* Mars 1971 burst-tested propellant vessel	18–19
Mariner Mars 1971 propulsion subsystem	22–26
Quality Assurance and Reliability	
Mariner Mars 1971 electronic parts control	19–22
Scientific Instruments	
gas chromatograph/mass spectrometer for *Viking* lander system	28–33
Solid-State Physics	
static test of *Mariner* Mars 1971 developmental test model	12–16
study of *Mariner* Mars 1971 burst-tested propellant vessel	18–19
Structural Engineering	
Mariner Mars 1971 propulsion support structure	7–11
static test of *Mariner* Mars 1971 developmental test model	12–16
modal survey for mathematical model of *Mariner* Mars 1971 spacecraft	16–17
Mariner Mars 1971 spacecraft overturning moment for longitudinal low-frequency environmental vibration test	17–18
Mariner Mars 1971 propulsion subsystem	22–26
configuration of *Viking* orbiter system	35–39
Television	
Mariner Mars 1971 television subsystem	3–7
Temperature Control	
Mariner Mars 1971: thermal resistance at chassis–subchassis interface	11–12
Viking orbiter system electronics temperature control	39–41
Viking orbiter system temperature control with solar energy controllers	41–43
Test Facilities and Equipment	
Mariner Mars 1971 television subsystem breadboard	3–7

Subject	Pages
Viking Project	
project description and status	27–28
gas chromatograph/mass spectrometer for lander system	28–33
effects of propellant slosh dynamics on orbiter system powered-flight control	33–35
configuration of orbiter system	35–39
orbiter system cabling and electronic equipment layout	39–41
orbiter system electronics temperature control	39–41
orbiter system temperature control with solar energy controllers	41–43

NASA — JPL — Coml., L.A., Calif.